Resource

Developmental Cell

Characterization of the human fetal gonad and reproductive tract by single-cell transcriptomics

Graphical abstract

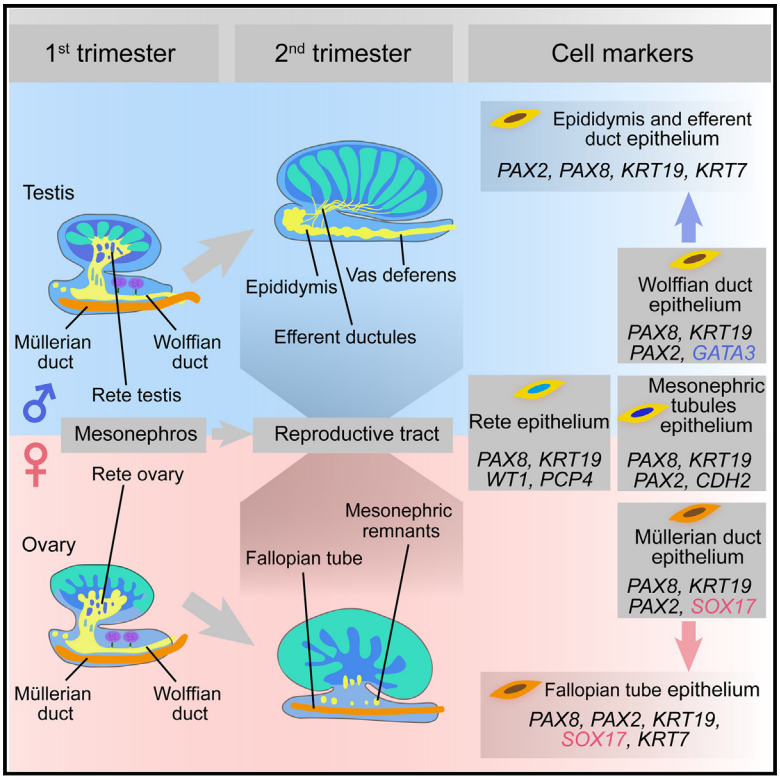

Highlights

- Pronounced sex differences emerge in the reproductive tract in the first trimester
- Key genes in the early reproductive tract associate with urogenital diseases
- The human rete testis and rete ovarii share common features in the first trimester
- Stromal and epithelial signatures diverge in gonads and adjacent reproductive tract

Authors

Jasin Taelman, Sylwia M. Czukiewska, Ioannis Moustakas, ..., Hailiang Mei, Xueying Fan, Susana M. Chuva de Sousa Lopes

Correspondence

x.fan@lumc.nl (X.F.), lopes@lumc.nl (S.M.C.d.S.L.)

In brief

Using single-cell transcriptomics and extensive validation by immunofluorescence, Taelman and Czukiewska et al. examine the development of fetal human gonads and the adjacent reproductive tract of both sexes during the first and second trimesters, identifying morphological and molecular changes as well as conserved and sex-specific features during differentiation.

Taelman et al., 2024, Developmental Cell *59*, 529–544
February 26, 2024
https://doi.org/10.1016/j.devcel.2024.01.006

CellPress

Developmental Cell

CellPress
OPEN ACCESS

Resource

Characterization of the human fetal gonad and reproductive tract by single-cell transcriptomics

Jasin Taelman,[1,6] Sylwia M. Czukiewska,[1,6] Ioannis Moustakas,[2] Yolanda W. Chang,[1] Sanne Hillenius,[1] Talia van der Helm,[1] Lotte E. van der Meeren,[3,4] Hailiang Mei,[2] Xueying Fan,[1,7,*] and Susana M. Chuva de Sousa Lopes[1,5,7,8,*]

[1]Department of Anatomy and Embryology, Leiden University Medical Center, 2333 ZC Leiden, the Netherlands
[2]Sequencing Analysis Support Core, Leiden University Medical Center, 2333 ZC Leiden, the Netherlands
[3]Department of Pathology, Leiden University Medical Center, 2333 ZC Leiden, the Netherlands
[4]Department of Pathology, Erasmus Medical Center, 3015 GD Rotterdam, the Netherlands
[5]Department for Reproductive Medicine, Ghent University Hospital, 9000 Ghent, Belgium
[6]These authors contributed equally
[7]These authors contributed equally
[8]Lead contact
*Correspondence: x.fan@lumc.nl (X.F.), lopes@lumc.nl (S.M.C.d.S.L.)
https://doi.org/10.1016/j.devcel.2024.01.006

SUMMARY

During human fetal development, sex differentiation occurs not only in the gonads but also in the adjacent developing reproductive tract. However, while the cellular composition of male and female human fetal gonads is well described, that of the adjacent developing reproductive tract remains poorly characterized. Here, we performed single-cell transcriptomics on male and female human fetal gonads together with the adjacent developing reproductive tract from first and second trimesters, highlighting the morphological and molecular changes during sex differentiation. We validated different cell populations of the developing reproductive tract and gonads and compared the molecular signatures between the first and second trimesters, as well as between sexes, to identify conserved and sex-specific features. Together, our study provides insights into human fetal sex-specific gonadogenesis and development of the reproductive tract beyond the gonads.

INTRODUCTION

Although certain aspects of human germ cell development and the contribution of the gonadal somatic niche are now relatively well characterized, limited attention has been given to the mesonephros, which contains the precursor to the (male and female) reproductive tract, as well as to the gonadal rete region, an epithelial structure that comes to connect the seminiferous tubules to the efferent ducts of the epididymis in males.

During human development, the intermediate mesoderm gives rise to the urogenital ridges, which include both the bipotential gonads and adjacent mesonephros. The mesonephroi emerge approximately at 3 weeks post fertilization (WPF).[1–4] The bipotential mesonephros initially contains corpuscles (analogous to the renal glomerulus and Bowman's capsule), mesonephric secretory (proximal) and collecting (distal) tubules, mesonephric (efferent) tubules (MTs), the Wolffian duct (WD) (or mesonephric duct), and the Müllerian duct (MD) (or paramesonephric duct).[1,3,4] The WD also originates from the intermediate mesoderm and induces the formation of the MTs around 4 WPF. The MD forms by an invagination of the coelomic epithelium at 6 WPF, which extends caudally under the guidance of the WD.[5] The bipotential gonadal ridge emerges at 5–6 WPF on the ventral side of the mesonephros, where the coelomic epithelium becomes pseudostratified and invades the underlying intermediate mesoderm.[6] At 6 WPF, sex determination starts with the differential expression of the Y-linked gene *SRY* in males, which subsequently induces a series of sex-specific events in the gonads and mesonephros.[6]

The sex-specific development of the WD and MD is controlled by mesenchymal-epithelium interactions that are influenced by sex hormones.[7,8] In males, the WD is maintained, while the MD regresses. This is mediated by the expression of androgen receptor (AR) in the WD mesenchyme, which is regulated by testosterone and anti-Müllerian hormone (AMH), produced by Leydig cells and Sertoli cells, respectively.[9] In males, the cranial MTs that connect the WD to the rete testis become the efferent ducts, while the WD develops into the epididymal ducts, the vas deferens, and the seminal vesicle.[10,11]

In females, the MD is preserved, while the WD and MTs regress due to not only the absence of AMH and androgens but also the presence of WNT ligands and the expression of NR2F2 by the WD mesenchyme.[7,8] However, the remains of the MTs and WD remain visible (Gartner's duct and cysts) in the ovarian broad ligament.[5] In females, the MD develops into the fallopian tube (as well as the uterus and part of the vagina).[1,3,5]

The rete region is integral to gonadal development and functions in both sexes. In adult testes, the rete testis forms a crucial connection between the seminiferous tubes, containing the gonadal germ cell niche, and the extragonadal efferent ducts of the epididymis, developed from MTs early during development.[12–15] In contrast to males, the primary female intraovarian rete ovarii regresses over time, leaving a few tubules in the hilus of the adult ovary.[16,17] However, cells from the rete ovarii have been associated with the origin of theca cell progenitors and the ovarian lymphatic vasculature,[18] as shown in mice.[19,20]

Studies in mice have described cells in the rete testis as having both mesonephric and Sertoli-like characteristics.[11,15] It has thus been suggested that the rete network consists of cell types from both origins, making it difficult to identify the molecular markers that define this region. Recently, Kulibin and Malolina investigated rete testis formation in mice between embryonic day (E)11.5 and E16.5.[21] In mice, rete testis cells express PAX8 (marker of MTs), as well as SOX9 and WT1 (Sertoli cell markers). At E13.5, PAX8+ SOX9+WT1+AMH−DMRT1− rete testis cells become canalized and form the rete cords, connected to the seminiferous tubes containing PAX8−SOX9+WT1+AMH+DMRT1+ Sertoli cells. From E14.5 to E16.5, the AMH+ cells near the rete cords are gradually replaced by PAX8+ rete cells.[21] During this period, this border region comprises a mixed population of PAX8+DMRT1+ and PAX8+DMRT1− cells.[13,21]

In mice, single-cell transcriptomics has been applied to investigate the developmental stages and cellular trajectories during male gametogenesis,[22,23] providing the molecular identity of the rete testis. Similarly, single-cell transcriptomics in humans has been used to study gametogenesis during fetal and adult life.[24–30] More recently, Garcia-Alonso and colleagues mapped human gonadal cells from 6 to 21 WPF and identified two subsets of PAX8+ rete cells: early PAX8+ rete cells that remain sexually undifferentiated at 6–8 WPF and late PAX8+ rete cells that emerge after 8 WPF.[31] In addition, adult human oviduct, and adult human proximal epididymis have also been profiled using single-cell transcriptomics.[32,33] However, the molecular signatures of human fetal mesonephroi and developing reproductive tract have not been investigated. As abnormal development of rete testis, WD, and MD is associated with infertility and urogenital disorders, mapping the development of the fetal rete and reproductive system by single-cell transcriptomics can help identify key players in disease phenotypes, as well as structural development.[8]

In this study, we performed single-cell transcriptomics on first trimester (1T) and second trimester (2T) human fetal male and female gonads, mesonephroi, and associated reproductive tracts. We focused on the characterization of the cells in the rete, WD, and MD and identified molecular features associated with sex-specific development and morphogenesis in humans.

RESULTS

Human fetal rete testis expresses PAX8 and KRT19 and can contain germ cells

To investigate rete testis development, we collected human fetal male gonads and mesonephroi/epididymis from both 1T (6–8 WPF, n = 4) and 2T (16–20 WPF, n = 7). According to previous studies, PAX8 and KRT19 were specifically expressed in human adult rete testis[34,35]; therefore, we first confirmed the expression of PAX8 and KRT19 in the human rete testis in the 1T (6–8 WPF, n = 4) and 2T (16–20 WPF, n = 7) (Figures 1A and 1B). At 6–6.5 WPF (n = 2), a group of PAX8+ cells close to the mesonephros marked the formation of the rete testis, whereas KRT19 formed a gradient from the coelomic epithelium toward the mesonephros (Figure S1A). At 8 WPF (n = 2), the rete testis, expressing PAX8 and KRT19, was not properly organized in tubules, in contrast to the well-organized AMH+ Sertoli cells in the seminiferous tubes (Figures 1A and 1B). Surprisingly, both DDX4+ germ cells (Figure 1A) and POU5F1+ germ cells (Figure 1B) were observed in the rete testis. Interestingly, at 8 WPF, we observed a striking PAX8+KRT19+ tubule with a central lumen inside of the testis in the region where future efferent ducts of the epididymis would form (Figures 1A and 1B). Furthermore, at 8 WPF, we noted the presence of germ cells at the basal part of the tubule (Figure 1B), as well as under the coelomic epithelium of the testis (Figures 1A, 1B, and S1B). At 16–20 WPF (n = 7), the PAX8+KRT19+ rete testis formed a well-defined network of tubules that connected with the seminiferous tubes (containing the AMH+ Sertoli cells) and still contained many DDX4+ germ cells (Figure 1A). Regarding the mesonephroi at 6–8 WPF, the MTs, WD, and part of the outer layer of the mesonephric corpuscle (particularly adjacent to the secretory tubules) were PAX8+KRT19+ as were the efferent tubules and the tubules in (the head of) the epididymis at 16–20 WPF (n = 7) (Figures 1A, 1B, and S1A). By contrast, the secretory tubules at 6–8 WPF (n = 4) were not only PAX8+KRT19+ but also AMH+ (Figures 1A, 1B, and S1A). Finally, the coelomic epithelium at 6–8 WPF (n = 4) and 16–20 WPF (n = 7) expressed low levels of PAX8 and high levels of KRT19 (Figures 1A and 1B).

Identification of main cell types in human fetal testis and male reproductive tract

Next, we isolated both fetal male and female gonads and associated reproductive tract tissue and performed single-cell transcriptomics (Figure 1C). A total of 31,749 cells from 12 different male donors from 7 to 18 WPF (10,096 cells from 1T and 21,653 cells from 2T) passed our quality control after removing doublets and correcting for batch effects and 19 distinct (male) clusters (mCL0–mCL18) were identified and visualized on a two-dimensional plot using uniform manifold approximation and projection (UMAP) (Figures 2A and S1C–S1E). Thereafter, the differentially expressed genes (DEGs) for each cluster were calculated (Table S1). According to cell identity annotation and known marker genes,[26,27,31,36,37] we confirmed that mCL2, mCL6, and mCL14 were Sertoli cells (*AMH*+*SOX9*+*GATM*+*DMRT1*+); mCL15 was endothelial cells (*PECAM1*+); mCL18 was smooth muscle cells (*RGS5*+); mCL16 was a mixed population of germ cells (*POU5F1*+ and/or *DDX4*+) and immune cells ($CD53^+$); mCL11 was epithelial rete testis (*PAX8*+*KRT19*+*PCP4*+); mCL1, mCL7, and mCL17 were epithelial cells from mesonephroi/epididymis (*EPCAM*+*ANXA2*+); and mCL0, mCL3, mCL5, mCL8, mCL12, and mCL13 were stromal cells from mesonephroi/epididymis (*NR2F2*+*DLK1*+*PDGFRA*+*ARX*−*GATA4*−), whereas mCL4, mCL9, and mCL10 were stromal cells from the testis (*NR2F2*+*DLK1*+*PDGFRA*+*ARX*+*GATA4*+) (Figures 2, 3, and S2A; Table S1). In particular, mCL9 contained Leydig cells (*CYP17A1*+*INSL3*+), mCL7 included epithelial cells of the MTs and WD (*LHX1*+*PAX2*+), and mCL1

CellPress
OPEN ACCESS

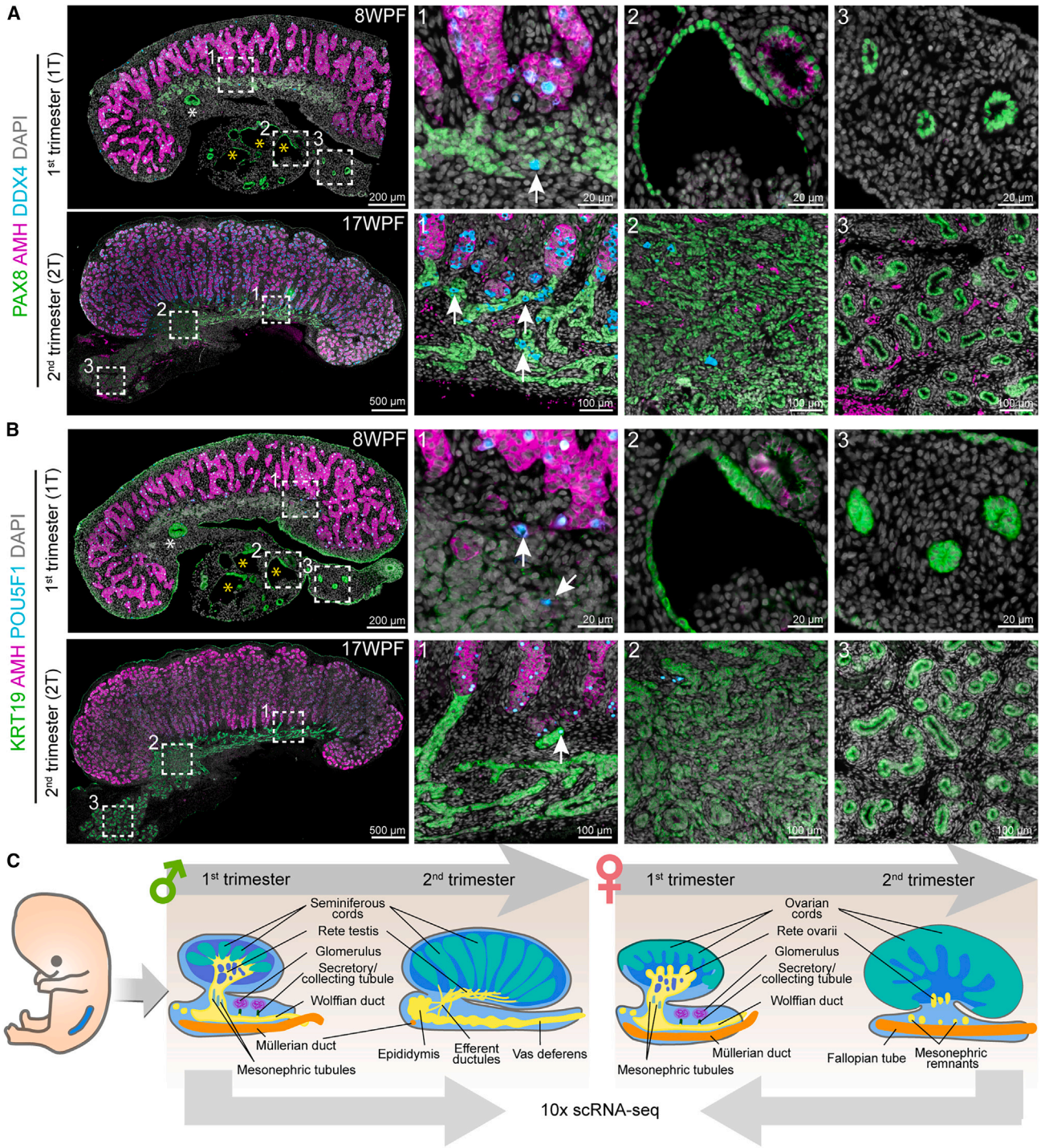

Figure 1. PAX8 and KRT19 expression in the fetal male testes and study setup

(A) Immunofluorescence for PAX8, AMH, and DDX4 in first trimester (6–8 WPF, n = 4) (top) and second trimester (16–20 WPF, n = 7) testes (bottom). White dashed boxes in left image indicate selected magnified regions on the right. In top left panel, white asterisk indicates PAX8+ tubule in testis, while yellow asterisks in top left panel indicates mesonephric corpuscles. White arrows indicate germ cells in rete testis.

(B) Immunofluorescence for KRT19, AMH, and POU5F1 in first trimester (6–8 WPF, n = 4) (top) and second trimester (16–20 WPF, n = 7) testes (bottom). White dashed boxes in left image indicate selected magnified regions on the right. In top left panel, white asterisk indicates KRT19+ tubule in testis and yellow asterisks in top left panel indicates mesonephric corpuscles. White dashed boxes in left image indicate selected magnified regions on the right. White arrows indicate germ cells in rete testis.

(C) Study setup.

See also Figure S1.

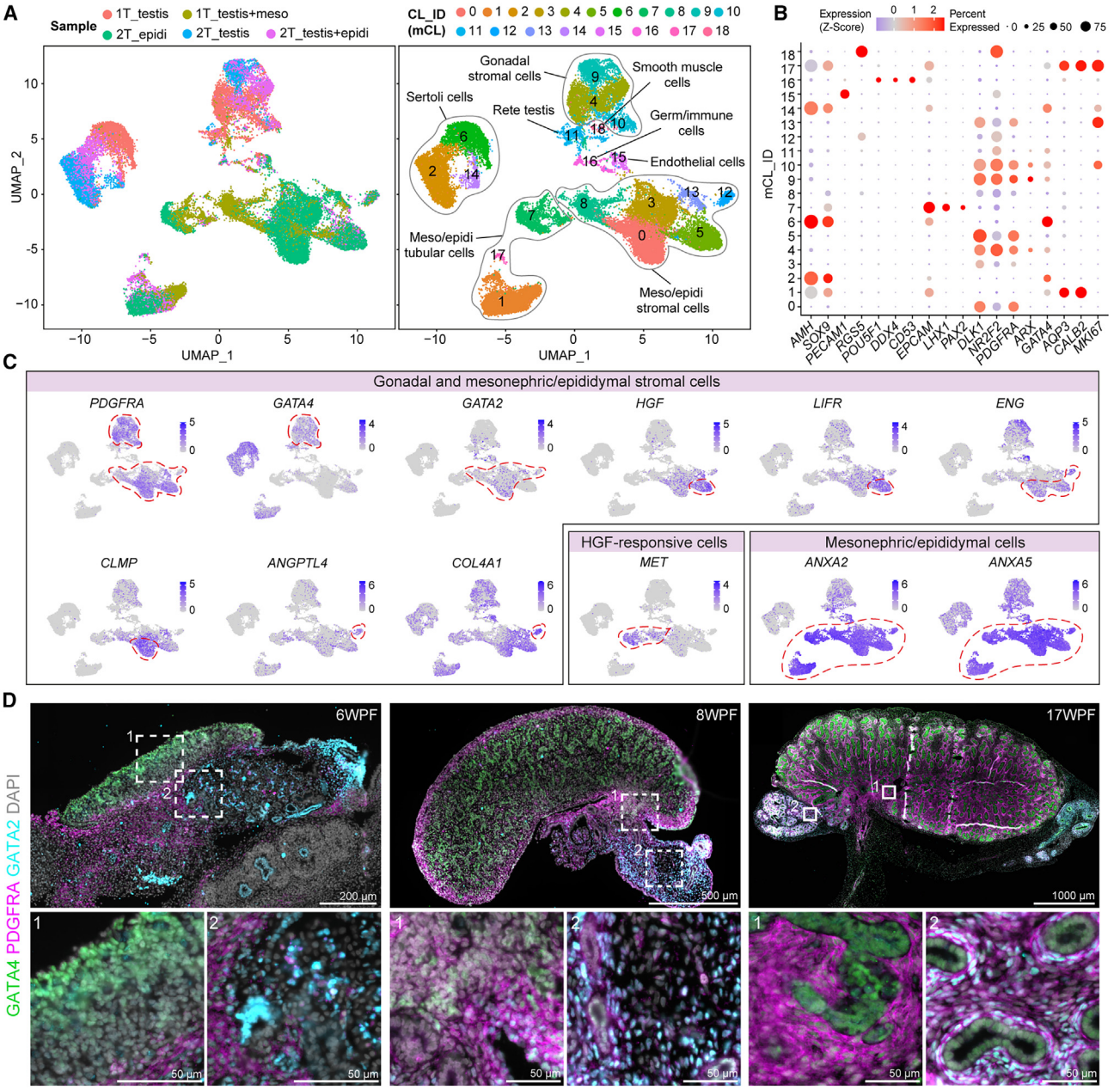

Figure 2. Molecular characterization of cell types in the human fetal male gonad and reproductive tract

(A) Uniform manifold approximation and projection (UMAP) plot showing the sample type and age (left) and cell clusters (mCL) obtained (right) for human fetal male gonad and reproductive tract.

(B) Dot plot showing the scaled expression (*Z* score) of genes of interest for male cell cluster identification.

(C) UMAP plot showing the expression of genes of interest to identify gonadal and mesonephric/epididymal (stromal) cells and HGF-responsive cells. Red dashed circles indicate cell populations of interest.

(D) Immunofluorescence for GATA4, PDGFRA, and GATA2 in testis and mesonephros at 6–6.5 WPF (n = 2) (left) and 8 WPF (n = 2) (middle) and testis and epididymis at 16–20 WPF (n = 7) (right). White dashed boxes indicate selected magnified regions (bottom).

See also Figures S1 and S2 and Table S1.

included cells from secretory tubules (*AQP3*+*CALB2*+ *GJA1*+ *CDH2*+*AMH*+) (Figure S2A). Interestingly, we identified clusters of proliferating (*MKI67*+) Sertoli cells (mCL14), gonadal stromal cells (mCL10), and mesonephric/epididymal stromal cells (mCL13) (Figure S2A).

Transcriptional analysis of the male stromal compartment

We identified complementary expression patterns for *GATA4*/GATA4 (positive in gonadal stromal cells and negative in mesonephric/epididymal stromal cells) and *GATA2*/GATA2 (negative

CellPress
OPEN ACCESS

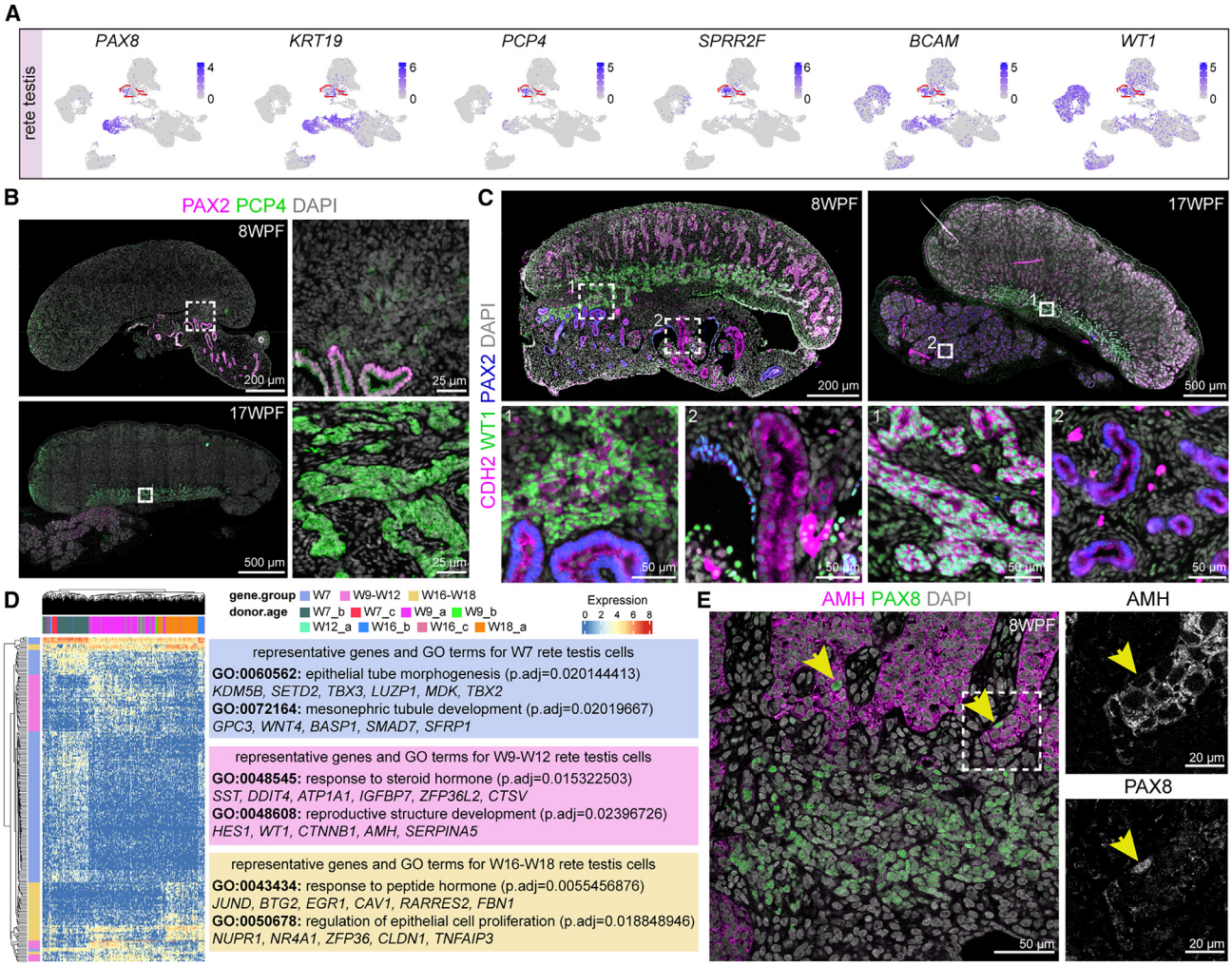

Figure 3. Transcriptional analysis during human fetal rete testis development

(A) Uniform manifold approximation and projection (UMAP) plot showing the expression of selected genes expressed in rete testis. Red dashed circles indicate mCL11.

(B) Immunofluorescence for PAX2 and PCP4 in testis and mesonephros at 8 WPF (n = 2) (top) and testis and epididymis at 16–20 WPF (n = 7) (bottom).

(C) Immunofluorescence for CDH2, WT1, and PAX2 in testis and mesonephros at 8 WPF (n = 2) (left) and testis and epididymis at 16–20 WPF (n = 7) (right). White dashed boxes in top image indicate selected magnified images (bottom).

(D) Heatmap showing differentially expressed genes in rete testis between three age groups 7, 9–12, and 16–18 WPF and associated representative GO terms (biological processes).

(E) Immunofluorescence for AMH and PAX8 in testis at 8 WPF (n = 2). Yellow arrows indicate PAX8+AMH+ cells in seminiferous tubules. White dashed boxes in left image indicate selected magnified region on the right showing separated channels.

See also Figure S3 and Table S2.

in gonadal stromal cells and positive in mesonephric/epididymal stromal cells) at 6–20 WPF (6–8 WPF, n = 4; 16–20 WPF, n = 7) (Figures 2C, 2D, and S2B). As expected, *NR2F2*/NR2F2 and *PDGFRA*/PDGFRA were expressed in both gonadal and mesonephric/epididymal stromal compartments at 6–20 WPF (Figures 2C, 2D, and S2). Interestingly, at 8 WPF (n = 2), PDGFRA clearly marked the tunica albuginea, whereas at 6–6.5 WPF (n = 2), PDGFRA was only observed anteriorly between the gonad and the mesonephros (Figure 2D); perhaps this is the zone that gives rise to the tunica. Furthermore, we noticed that calcium-binding annexin family members (ANXAs) such as *ANXA1*, *ANXA2*, *ANXA3*, and *ANXA5* were highly expressed in cells from the mesonephroi/epididymis but lowly expressed in cells from the testis (Figures 2C and S2A).

mCL5 showed high expression of *HGF* and *LIFR* (Figure 2C). *HGF* is known to be involved in epithelial-mesenchymal crosstalk,[38] and we observed the expression of its receptor *MET* in mCL7 and mCL8 (Figure 2C); hence, mCL5 may correspond to mesenchymal cells that regulate the organization of the mesonephroi/epididymal tubule network. Furthermore, *ENG* was expressed in mesonephric stromal cells in mCL0, mCL5, and mCL12, but not in mCL3. Cells from mCL0 could be distinguished by the relatively elevated expression of cell adhesion protein *CLMP*, while mCL12 showed marked expression of

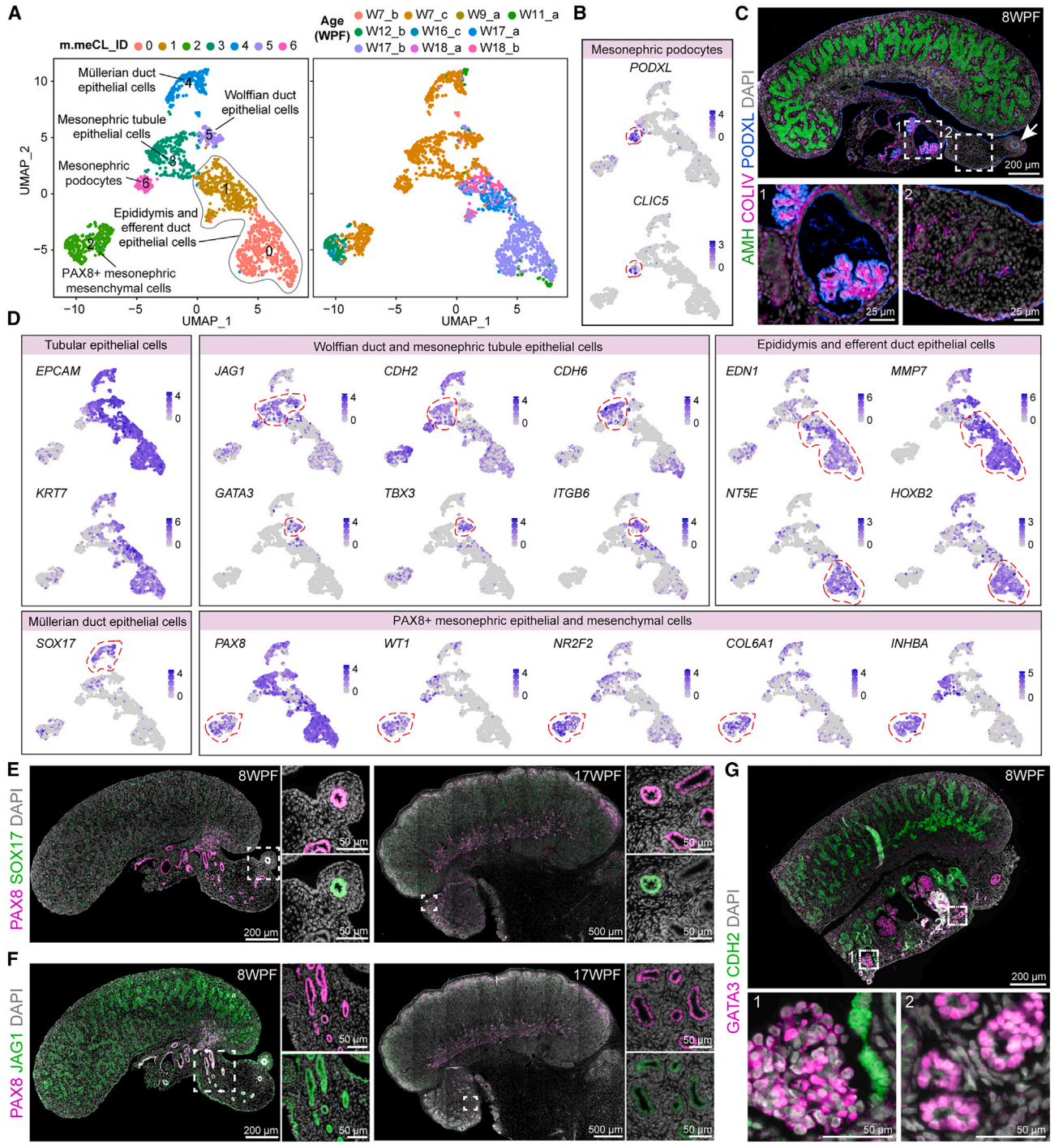

Figure 4. Molecular characterization of cell types in human fetal male mesonephros and epididymis

(A) Uniform manifold approximation and projection (UMAP) plot showing cell cluster identity (m.meCL) (left) and age/donor (right) obtained by sub-clustering mCL7.

(B) UMAP plot showing the expression of selected markers for mesonephric podocytes. Red dashed circles indicate cell populations with specific marker expression.

(C) Immunofluorescence for AMH, COLIV, and PODXL in testis and mesonephros at 6–8 WPF (n = 4). White dashed boxes indicate selected magnified regions (bottom).

(D) UMAP plot showing expression of genes of interest to identify different populations of tubular epithelial cells and mesenchymal cells. Red dashed circles indicate cell populations of interest.

(legend continued on next page)

ANGPTL4 and *COL4A1* (Figure 2C). Taken together, we identified different populations of male mesonephric/epididymal stromal cells, suggesting that mCL0, mCL5, and mCL12 may be associated with mesonephric/epididymal tubule organization and vascularization.

Transcriptional analysis of fetal rete testis cells

Cells from mCL11 co-expressed *PAX8*/PAX8, *KRT19*/KRT19, *PCP4*/PCP4, *CDH2*/CDH2, and *WT1*/WT1 and corresponded to the rete testis (Figures 1A, 1B, and 3A–3C). Interestingly, at 6–6.5 WPF (n = 2), PCP4 was still absent from the forming rete testis, whereas WT1 was already expressed (Figures S3A and S3B). PAX2 was consistently absent from the rete testis but was strongly expressed in the tubules of the mesonephroi/epididymis (Figures 3B and S3A). We observed that WT1+ CDH2+ cells from rete testis extended into the mesonephros and were in close proximity with PAX2+CDH2+ MTs (efferent) at 8 WPF (n = 2) (Figure 3C). In agreement with the transcriptomics data, CDH2 was strongly detected in secretory tubules at 8 WPF, whereas the PAX2 expression was low (Figures 2B, 3C, and S2A).

To further explore rete testis development between 1T and 2T, the cells from mCL11 were further sub-clustered (Figure S3C). Sub-clusters of mCL11 included cells of the coelomic epithelium (*UPK3B+KRT19+*) and proliferating cells (*MKI67+*) (Figure S3D); therefore, we excluded those from further analysis. We focused only on bona fide rete testis cells (*PAX8+UPK3B−MKI67−*) aged 7–18 WPF (CL0, CL2, and CL3) (Figures 3D and S3E) and calculated DEGs to differentiate between three age groups: 7 , 9–12, and 16–18 WPF. We extracted 234 DEGs in total for these three groups (Table S2). Gene Ontology (GO) term enrichment analysis showed that DEGs for 7-WPF rete testis were involved in "epithelial tube morphogenesis" and "MT development" (Figure 3D). Notably, WNT4 was recently reported to play a crucial role in the formation of mouse rete testis[23]; our results suggested that WNT signaling may also be important for early human rete testis development. DEGs for 9–12 and 16–18 WPF were associated with "response to steroid hormone" and "response to peptide hormone" (Figure 3D). This is in line with tubule formation at 2T and the known role of rete testis in steroid hormone pathway.[10]

It was recently demonstrated in mouse that PAX8+ cells contribute to Sertoli and pre-granulosa cell pools.[23] In agreement, we observed that AMH+PAX8+ cells or GATM+PAX8+ cells were present at the developing interface between the rete testis and the seminiferous tubes in 8-WPF testis (n = 2) (Figures 3E and S3F).

Transcriptional analysis of the male mesonephroi and epididymal tubular compartment

We investigated the transition from male mesonephros (m.me) into epididymis, regarding (male) m.WD, m.MTs, and m.MD, by sub-clustering tubular epithelial cells from mCL7 (and excluding mCL1 that included tubular epithelial cells from secretory/collecting tubules) (Figures 2A and 4A). We retained 1,817 cells (from 10 different donors from 7 to 18 WPF), obtained 7 different clusters (m.meCL0–m.meCL6) (Figure 4A), and calculated the DEGs for each m.meCL (Table S3).

The m.meCL6 (male mesonephric podocytes) showed cells with similarities to nephric podocytes (*PODXL+CLIC5+*)[37] (Figure 4B). Using immunofluorescence, we confirmed the presence of PODXL+ podocytes as well as PODXL+ cells in the outer layer of the corpuscle, vascular endothelial cells, the coelomic/surface epithelium of the mesonephros, and the m.MD, but not in the m.MTs at 6–8 WPF (n = 4) (Figure 4C).

Recently, SOX17 has been described as a marker of epithelial cells in the human adult fallopian tube and that it derives from the (female) f.MD; it has been suggested that SOX17 and PAX8 could drive the differentiation of the fallopian tube epithelium.[39] In our dataset from male mesonephroi/epididymis, *SOX17* was specifically expressed in m.meCL4 (m.MD) (Figure 4D). Immunofluorescence for SOX17 showed the expression in the m.MD in the male mesonephros at 6–8 WPF (n = 4) and the regressing m.MD in the epididymis of 16–20 WPF (n = 7) testis (Figures 4E and S3G).

Cells in m.meCL3 and m.meCL5 were mostly from 1T and showed high expression of *JAG1*, suggesting that they may correspond to the m.WD and m.MTs.[40] JAG1 was highly expressed in the m.WD and m.MTs at 6–8 WPF (n = 4) and was moderately expressed in m.WD and m.MTs at 16–20 WPF (n = 7) (Figures 4F and S3H). Specifically, m.meCL5 (m.WD) expressed high levels of *KRT7*, *GATA3*, *TBX3*, and *ITGB6*, whereas m.meCL3 (m.MTs) expressed high levels of *CDH2* and *CDH6*, suggesting that they may represent epithelial cells of m.WD and m.MTs, respectively (Figures 4D and 4G).

Cells in m.meCL0 and m.meCL1 (male epididymis and efferent duct epithelial cells) expressed *EDN1* and *MMP7* (Figure 4D). *EDN1* is expressed in human efferent and epididymal ducts,[41] whereas *MMP7* is involved in epididymal coiling and segmentation of the caput region,[42,43] strongly suggesting that cells in m.meCL0 and m.meCL1 were epididymis/efferent duct epithelial cells that were mainly from 2T. Moreover, cells in m.meCL0 showed high expression of *NT5E* and *HOXB2* (Figure 4D). *NT5E* was detected in the cauda epididymis in mouse,[44] and *HOXB2* was expressed in rat epididymis, showing higher expression in corpus/caudal epithelial cells than in the caput region.[45] Taken together, the molecular signature associated with m.meCL1 may correspond to the caput region of the epididymis and efferent ducts, while that associated with m.meCL0 may correspond to the corpus and caudal region of the epididymis.

To examine the differences between m.WD and m.MTs from 1T (m.meCL3 + m.meCL5) and the epididymis and efferent duct cells from 2T (m.meCL0 + m.meCL1), we calculated DEGs between the two groups and performed GO enrichment

(E) Immunofluorescence for PAX8 and SOX17 in testis and mesonephros at 6–8 WPF (n = 4) (left) and testis and epididymis at 16–20 WPF (n = 7) (right). White dashed boxes indicate selected magnified regions (right).
(F) Immunofluorescence for PAX8 and JAG1 in testis and mesonephros at 6–8 WPF (n = 4) (left) and testis and epididymis at 16–20 WPF (n = 7) (right). White dashed boxes indicate selected magnified regions (right).
(G) Immunofluorescence for GATA3 and CDH2 in testis and mesonephros at 8 WPF (n = 2). White dashed boxes indicate selected magnified regions (bottom).
See also Figure S3 and Table S3.

analysis, identifying different sets of genes involved in similar GO terms, such as "reproductive structure development" and response to steroid hormones (Figure S3I).

Intriguingly, cells in m.meCL2 (male PAX8+ mesonephric mesenchymal cells) lacked *EPCAM* but expressed mesenchymal markers, such as *WT1*, *NR2F2*, and *COL6A1*, as well as *INHBA* (Figure 4D). In mice, *INHBA* was restricted to the mesenchyme and involved in activin-induced epithelial coiling of the anterior m.WD.[46] Notably, m.WD failed to elongate and coil in *INHBA*-deficient mice.[47] This suggested that a group of *PAX8*+ mesenchymal cells may participate in the mesenchyme-epithelium interaction and morphogenesis of the epididymis.

Identification of main cell types in human fetal ovary and female reproductive tract

We investigated the molecular signature of the cells in the female gonad, as well as in the mesonephros and fallopian tube (Figure 1C) to determine the differences and similarities between the sexes. In total, 21,049 female cells (from 11 donors aged 6–18 WPF; 10,284 cells from 1T and 10,765 cells from 2T) passed our quality control thresholds (Figures 5A, 5B, and S4A–S4C). Using a Seurat-based analysis, we identified 15 distinct (female) clusters (fCL0–fCL14) (Figure 5A), and the DEGs for each cluster were calculated (Table S4). On the basis of the DEGs and several known marker genes,[27,31,36,37] we identified the cells in fCL5 and fCL12 as coelomic/ovarian surface epithelium (*UPK3B*+*KRT19*+*WT1*+*EPCAM*−); in fCL4 and fCL9 as pre-granulosa cells (*FOXL2*+*GATM*+*WT1*+); in fCL11 as smooth muscle cells (*RGS5*+); in fCL10 as endothelial cells (*PECAM1*+); in fCL14 as immune cells (CD53+); in fCL8 as fetal germ cells (*POU5F1*+ or *DDX4*+); in fCL7 as tubular cells of the f.MTs, f.MD, and f.WD (*EPCAM*+*LHX1*+*PAX2*+); in fCL13 as mesonephric podocytes (*PODXL*+*CLIC5*+); and in fCL2 as secretory tubules and mesonephric remnant cells (*GJA1*+*CDH2*+*AQP3*+*CALB2*+) (Figures 5B and S4D–S4F).

As in males, female stromal cells expressed *PDGFRA*/PDGFRA (fCL0, fCL1, fCL3, and fCL6), and the expression of *GATA2*/GATA2 and *GATA4*/GATA4 was sufficient to distinguish gonadal stromal cells in fCL3 (*PDGFRA*+*GATA4*+*ARX*+) from mesonephric/fallopian tube stromal cells in fCL0 and fCL1 (*PDGFRA*+*GATA2*+), validated at 8–20 WPF (8–12 WPF, n = 2; 15–20 WPF, n = 3) (Figures 5C and S4D). Cells in fCL6 were proliferating stromal cells (*PDGFRA*+*MKI67*+) (Figure S4D). We noticed that *SULT1E1*, which encodes for an estrogen sulfotransferase and has been associated with hormone-dependent tissues such as the testis and endometrium,[48] was particularly expressed in fCL1 (Figure S4D). Expression of SULT1E1 was detected exclusively in mesonephros stromal cells at 8–12 WPF (n = 2). As the mesonephros developed, more SULT1E1− stromal cells emerged, and SULT1E1 became more restricted to stromal cells surrounding the MD and the remnants of the MTs at 20 WPF (Figure 5D). SULT1E1 was also highly expressed in mesonephric/epididymal stromal cells in males from 6 to 20 WPF (n = 11) and to some extent in the stromal compartment of the rete testis (Figure 5E). Immunofluorescence for WT1 confirmed high expression in the ovarian surface epithelium cells and GATM+ pre-granulosa cells at 8–20 WPF (8–12 WPF, n = 2; 15–20 WPF, n = 3) (Figure S5A). Similar to males, *ANXA2* and *ANXA5* were also strongly expressed in the female mesonephros, compared with the ovary, with *ANXA1* and *ANXA3* more prominent in fCL3 (f.MTs, f.WD, and f.MD) (Figures 6A and S4F).

When investigating the expression of identified male rete testis markers in the female dataset, we observed high expression of *PAX8*, *PCP4, BCAM*, and *SPRR2F*, but low *KRT19*, in a group of cells in fCL4 (pre-granulosa cells) that could correspond to female rete ovarii cells (Figures 6B and S4E). To further characterize these cells, we sub-clustered fCL4 and obtained 4 sub-clusters (G0 to G3) (Figures S5B and S5C). Within the sub-clusters, we identified the cells in G3 as (*PAX8*+) rete ovarii epithelial cells, the female equivalent to the male rete testis epithelial cells. These cells were present in female gonads from mainly 1T (Figures 6C and 6D). Validation by immunofluorescence for PAX8 and KRT19 showed a core of rete ovarii cells at 8–20 WPF (n = 5) that in contrast to males did not organize in tubules (Figures 6E, 6F, S5D, and S5E). Moreover, as in males, PAX8 and KRT19 were also strongly expressed in the f.MTs, f.WD, and f.MD in females (Figures 6E, 6F, S5D, and S5E).

Transcriptional analysis of female mesonephroi and fallopian tube tubular compartment

We extracted cells from fCL7 (female mesonephroi and fallopian tube tubular cells) from the female dataset and performed sub-clustering to obtain the molecular signature of the f.MTs, f.WD, and f.MD. We obtained 5 female mesonephric sub-clusters (f.meCL0 to f.meCL4) from 951 cells (Figure 6G) and calculated the DEGs (Table S5). In agreement with the molecular signature obtained in males, f.meCL3 corresponded to the f.WD (*GATA3*+), f.meCL2 corresponded to f.MTs (*CDH2*+*PCP4*+), f.meCL1 corresponded to the 1T f.MD (*SOX17*+*PCP4*+), and f.meCL0 were 2T fallopian tube epithelial cells (*SOX17*+*KRT7*+*CAV1*+) (Figure 6H).

Differential gene expression between the 1T f.MD (f.meCL1) and 2T fallopian tube epithelial cells (f.meCL0+f.meCL4) was calculated between the two groups, and the GO term enrichment identified "Wnt signaling pathway" in the 1T, in contrast to response to peptide hormone and "positive regulation of epithelial cell migration" in the 2T (Figure S5G).

We validated the expression of SOX17 and KRT7 in 1T f.MD as well as in 2T and 3T fallopian tube epithelial cells (8–12 WPF, n = 2; 15–20 WPF, n = 3; 30 WPF, n = 1) and uterine epithelial cells (developing endometrium) (13–19 WPF, n = 2; 30 WPF, n = 1) (Figures 6I, S5F, S6A, and S6B) and visualized the mutually exclusive expression of GATA3 and PCP4/CDH2 (Figure 6J). GATA3 was expressed in the f.WD; and PCP4/CDH2 were expressed in f.MTs (note that the outer layer of the corpuscle was also CDH2+PCP4+, but the secretory tubules were CDH2+PCP4−) (Figure 6J).

In the human embryo, not only the fallopian tube but also the uterus develops from the f.MD[1,3,5]; therefore, we also investigated the expression of several observed mesonephric epithelial and mesenchymal markers in the uterus during the 2T. In the uterus during 2T (13–19 WPF, n = 2), epithelial markers PAX8, PCP4, and PAX2 were expressed homogenously in the uterine epithelial lining (Figures S6B and S6C), whereas SULT1E1 and PDGFRA were expressed in the uterine mesenchyme (Figures S6D and S6E). In contrast to the 2T fallopian tube that

CellPress
OPEN ACCESS

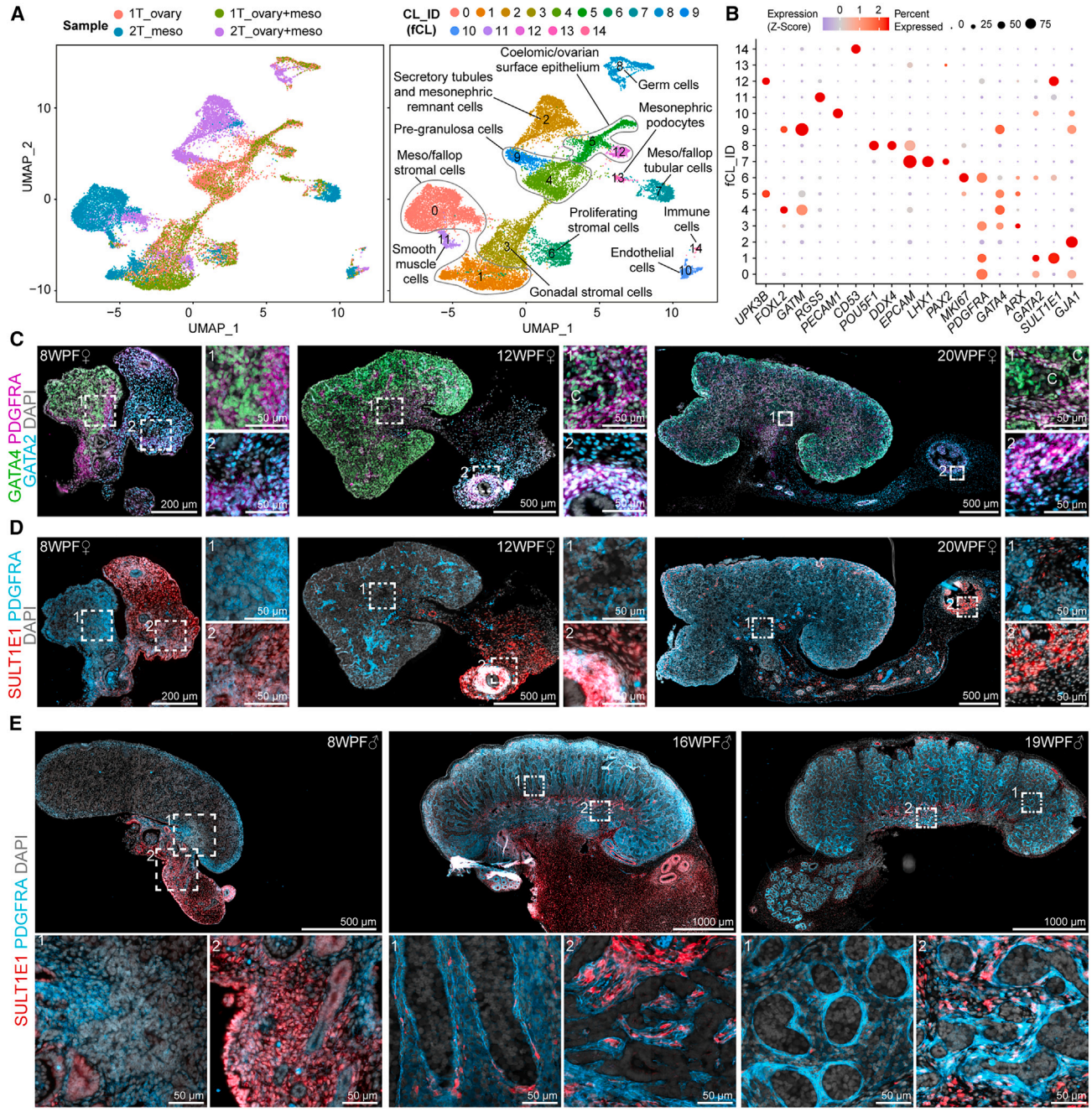

Figure 5. Molecular characterization of cell types in human fetal female gonad and reproductive tract

(A) Uniform manifold approximation and projection (UMAP) plot showing the sample type and age (left) and cell clusters (fCL) obtained (right) for human fetal female gonad and reproductive tract.

(B) Dot plot showing the scaled expression (*Z* score) of genes of interest for female cell cluster identification.

(C) Immunofluorescence for GATA4, PDGFRA, and GATA2 in ovary and mesonephros at 8 WPF (n = 1) (left) and in ovary and fallopian tube at 12 WPF (n = 1) (middle) and 15–20 WPF (n = 3) (right). White dashed boxes indicate selected magnified regions (left).

(D) Immunofluorescence for SULT1E1 and PDGFRA in ovary and mesonephros at 8 WPF (n = 1) (left) and in ovary and fallopian tube at 12 WPF (n = 1) (middle) and 15–20 WPF (n = 3) (right). White dashed boxes indicate selected magnified regions (left).

(E) Immunofluorescence for SULT1E1 and PDGFRA in testis and mesonephros at 8 WPF (left) and in (rete) testis at 16 WPF (middle) and 19 WPF (right) (6–20 WPF; n = 11). White dashed boxes indicate selected magnified regions (bottom).

See also Figure S4 and Table S4.

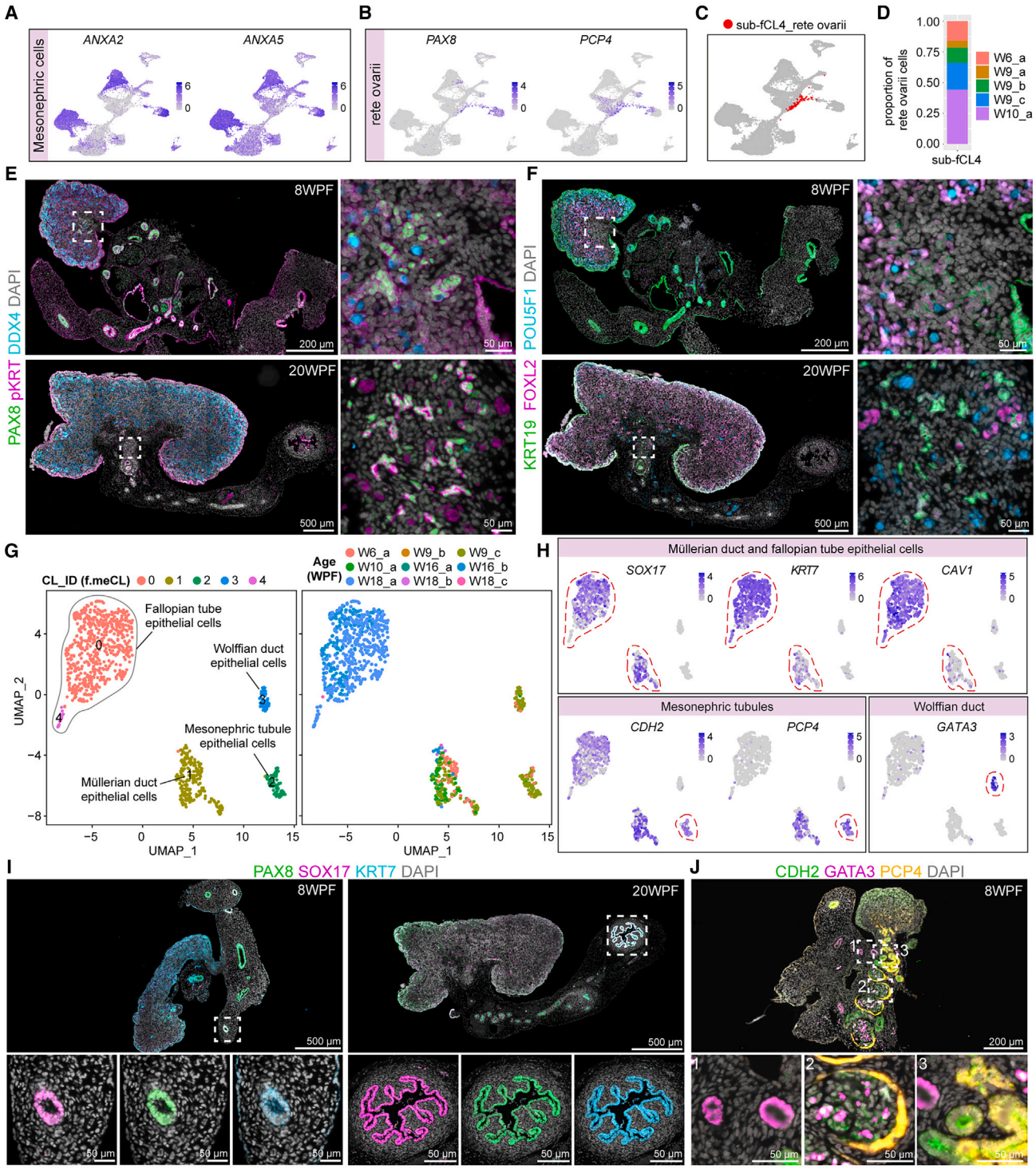

Figure 6. Identification of the rete ovarii and mesonephric female tubule cells

(A) Uniform manifold approximation and projection (UMAP) plot showing the selected mesonephric cell markers.

(B) UMAP plot showing the selected rete ovarii markers.

(C) UMAP plot showing the identified rete ovarii epithelial cells in the total female dataset.

(D) Bar plot showing the proportion of rete ovarii epithelial cells per donor.

(E) Immunofluorescence for pan (p)KRT, PAX8, and DDX4 in ovaries and mesonephros at 8 WPF and ovary and fallopian tube at 20 WPF (8–20 WPF; n = 5). White dashed boxes in overview image indicate the magnified region (right).

(legend continued on next page)

expressed neither GATA2 nor GATA4 in epithelial cells (Figure 5C), the 2T uterus (13–19 WPF, n = 2) expressed both GATA2 and GATA4 in the uterine mesenchyme as well as the epithelial lining (Figure S6E).

Comparison of the first trimester reproductive tract between sexes

To compare the molecular signature of the fetal rete epithelial cells between the sexes in the 1T, we first determined the gene expression differences in the 1T male dataset between rete testis (m.rete), m.WD, m.MTs, and m.MD, as well as gene expression differences in the 1T female dataset between rete ovarii (f.rete), f.WD, f.MTs, and f.MD (Figure 7A). We identified 68 DEGs upregulated in the 1T m.rete compared with the 1T male dataset (Table S6) and 79 DEGs upregulated in the 1T f.rete compared with the 1T female dataset (Table S7). We then intersected the two sets of 1T rete DEGs and obtained 32 commonly upregulated genes (Figures 7B and 7C), which included *PAX8*, *WT1*, *BCAM*, *SPRR2F*, and *PCP4*, as expected (Figures 3A, 3C, 6B, and S4E), as well as AMH receptor *AMHR2* and testicular apoptosis regulator gene *IGFBP3*.[49] The unique 1T male rete DEGs included *SST* and *ID2* (Figure S6F), whereas unique 1T female rete DEGs included *BMP4* (Figure S6G).

Next, we focused on similarities during early reproductive tract development in the 1T. After intersecting the six groups of obtained DEGs (f.WD, f.MD, f.MTs, m.WD, m.MD, and m.MTs), we obtained 25 genes that were conserved in the tubular structures in both sexes, including *PAX2*, *PAX8*, *LHX1*, *CD24*, and *EPCAM* (Figures 7D and 7E). These were associated with GO terms "positive regulation of epithelial cell differentiation" and "urogenital system development." Furthermore, we identified 28 + 6 DEGs that were shared between the WD of both sexes, but not by the MD (Figure 7F), whereas 10 DEGs were shared between the MD of both sexes, but not by the WD (Figure 7F). Common DEGs associated with WD included *FXYD2* and *GATA3*. *FXYD2* encodes a subunit of Na^+-K^+-ATPase involved in urine filtration (was also a common DEG in MTs of both sexes),[50] while *GATA3* encodes an effector of PAX2 and PAX8 in the regulation of WD morphogenesis.[51,52] Common DEGs associated with MD included *SOX17*, as expected,[39] and *FGF18*, which plays a role in uterine development[53,54] (Figure 7F).

To map emerging sex differences during early reproductive tract development in humans, we first filtered for DEGs shared between male reproductive tract (m.WD, m.MD, and m.MTs), but not by the female counterparts, and obtained 16 genes that included *LAMC2* and *TUBA4A* (Figure 7G). Next, we filtered for DEGs shared between female reproductive tract (f.WD, f.MD, and f.MTs), but not by the male counterparts, and obtained 15 genes that included *PDGFA*, which is important to the development of the female reproductive tract[55] (Figure 7G). Interestingly, when only unique DEGs were considered, male structures (m.WD, m.MD, and m.MTs) clustered together, while the female structures (f.WD, f.MTs, and f.MD) separated (Figure 7H), suggesting early sex differentiation of the f.MD. Finally, we pooled all the male-specific DEGs (m.WD, m.MD, and m.MTs) and obtained GO term enrichment for "epithelial cell migration," "response to estradiol," and "regionalization." By contrast, female-specific DEGs (f.WD, f.MD, and f.MTs) yielded GO term enrichment for "response to BMP," WNT signaling pathway, and reproductive structure development (Figure 7I). This suggested that female reproductive tract initiates sex-specific cell signaling already in the 1T, whereas the male reproductive tract is still undergoing morphogenesis and regionalization, likely through HOX gene expression (Figure 7I) as expected.[11]

Finally, we investigated whether the genes expressed in the tubular compartment of the reproductive tract (WD, MD, and MTs) during the 1T were associated with human diseases of the reproductive tract during adult life. For this, we intersected all female and male DEGs identified in the WD, MD, and MTs (Figure 7D) with genes related to "urogenital abnormalities," "genitourinary cancer," and "ambiguous genitalia" (Figures 7D and 7J). *PAX2*, *HNF1B*, *TGFB2*, and *GFRA1* were associated with urogenital abnormalities; *AR*, *ABCB1*, *CD44*, *WNT7A, TBC1D9, CXADR*, and *GSTP1* were associated with genitourinary cancer; and *AR*, *CYB5A*, *EFNB2*, *PSAT1*, *MAP3K1*, *TGIF1*, *SOX9*, *FREM2*, *POMC*, *AKR1C3*, and *PHGDH* were associated with ambiguous genitalia (Figure 7J). Interestingly, several genes were only expressed in the female or the male developing reproductive tract, indicating sex-specific involvement in these diseases. Together, the results provide molecular insights for human urogenital/reproductive tract development (Figures S7A and S7B) and relevant diseases.

DISCUSSION

The rete testis, mesonephros-derived efferent ducts, and epididymis together form a continuous tubular system that plays an essential role in the transport of the sperm cells[56] and hence male fertility. Similarly, during female development, the sex-specific differentiation of the MD is responsible for a functional female reproductive tract.[7] Here, we have investigated the transcriptomics landscape of male and female human fetal mesonephros and derived-reproductive tract and identified markers for specific structures and cell types. For example, we have shown that PCP4 and PAX8 were expressed in (male and female) rete epithelial cells, that SOX17 marked MD epithelial cells, and that mesonephric and nephric podocytes shared several markers (such as *PODXL* and *CLIC5*); in addition, we identified

(F) Immunofluorescence for POU5F1, KRT19, and FOXL2 in ovaries and mesonephros at 8 WPF and ovary and fallopian tube at 20 WPF (8–20 WPF; n = 5). White dashed box in overview image indicates the magnified region (right).
(G) UMAP plot showing the cell cluster identity (f.meCL) (left) and age/donor (right) obtained by sub-clustering fCL7.
(H) UMAP plot showing the expression of selected markers for mesonephric epithelial cells. Red dashed circles indicate cell populations with specific marker expression.
(I) Immunofluorescence for PAX8, SOX17, and KRT7 in ovary and mesonephros at 8 WPF and ovary and fallopian tube at 20 WPF (8–20 WPF; n = 5). White dashed boxes indicate selected magnified regions (bottom).
(J) Immunofluorescence for GATA3, PCP4, and CDH2 in ovary and mesonephros at 8 WPF (n = 1). White dashed boxes indicate selected magnified regions (bottom).
See also Figure S5 and Table S5.

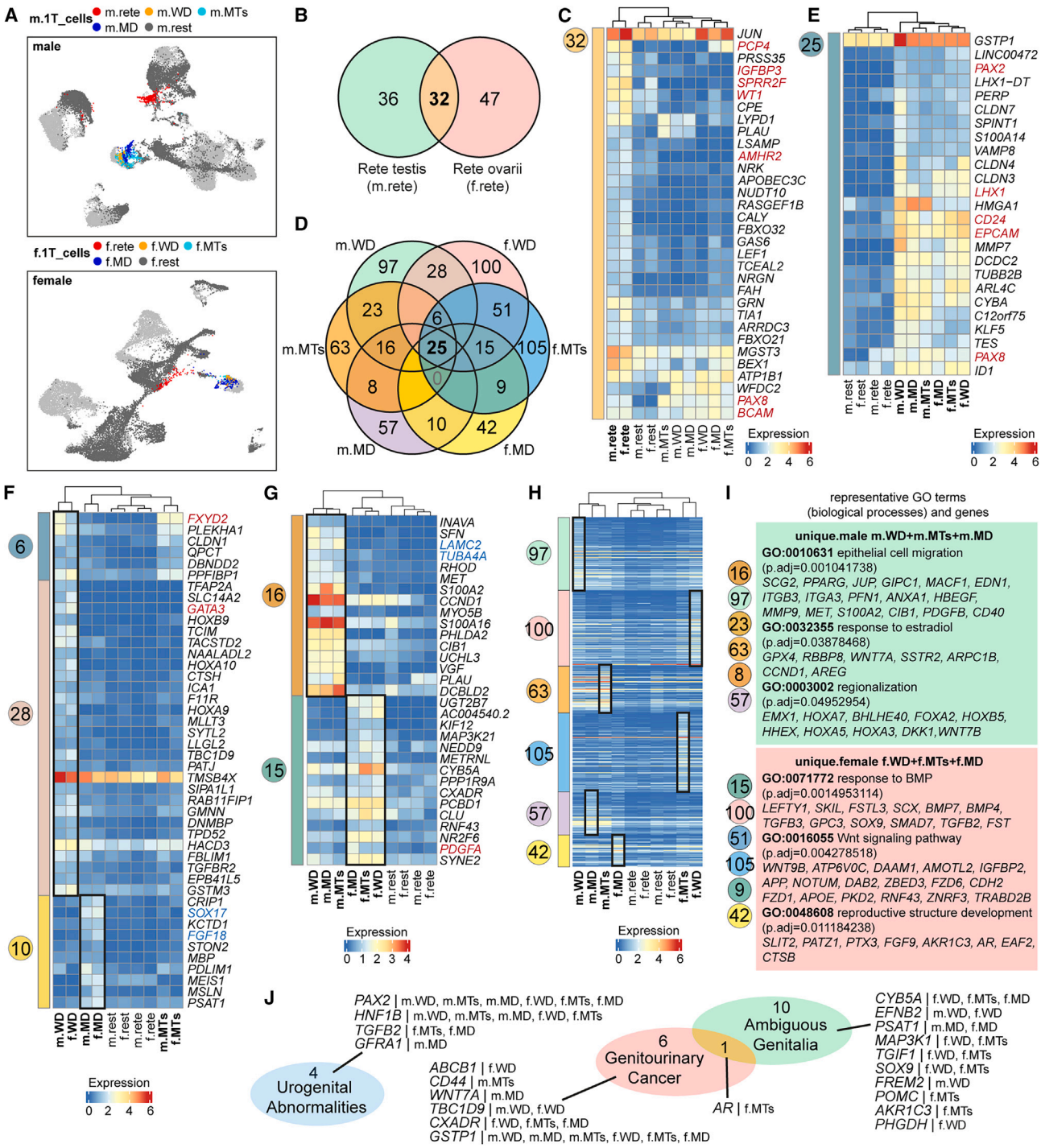

Figure 7. Transcriptional comparison of 1T rete, Wolffian duct, mesonephric tubules, and Müllerian duct between sexes

(A) Uniform manifold approximation and projection (UMAP) plots showing the complete male dataset (top) and female dataset (bottom) with highlighted 1T cells separated in main cell types of interest (rete, Wolffian duct [WD], Müllerian duct [MD], mesonephric tubules [MTs], and the rest).

(B) Venn diagram showing the intersection between DEGs in 1T rete ovarii epithelial cells and DEGs in 1T rete testis epithelial cells.

(C) Heatmap showing the mean expression of 32 DEGs conserved in the rete between sexes in 1T male and female cell types of interest.

(D) Venn diagram showing the intersection between the DEGs in 1T male and female cell types of interest (m.WD, m.MTs, m.MD, f.WD, f.MTs, and f.MD).

(E) Heatmap showing the mean expression of 25 DEGs conserved between m.WD, m.MTs, m.MD, f.WD, f.MTs, and f.MD in 1T male and female cell types of interest.

(F) Heatmap showing the mean expression of 28 DEGs conserved between m.WD and f.WD; 6 DEGs conserved between m.WD, m.MTs, f.WD, and f.MT; and 10 DEGs conserved between m.MD and f.MD in 1T male and female cell types of interest.

(legend continued on next page)

the population of mesonephric secretory cells in 1T characterized by *CDH2*+*AQP3*+*CALB2*+*PAX2*−. These early secretory cells already showed sex-specific differences because AMH was only expressed in male cells. Moreover, mesonephric cells can be distinguished from gonadal cells by the expression of ANXAs, especially *ANXA2* and *ANXA5*.

Surprisingly, we observed the presence of (POU5F1+ and or DDX4+) germ cells in the rete tubules. The transcriptional profile of germ cells in human fetal gonadal cells has been extensively mapped and analyzed,[26,27,31] and our analysis regarding germ cells largely confirmed previous findings. The gonadal niche interstitial cells at 6–7 WPF, described as a bipotential progenitor population, in males can still give rise to Sertoli cells, fetal Leydig cells, and interstitial lineages[26] and in females can generate pre-granulosa cells in two separate waves (a second wave taking place after 11 WPF).[31] In agreement, pre-granulosa cells from 6 to 10 WPF and from 10 to 18 WPF showed different molecular signatures.

Our analysis of the rete testis confirmed recent results in both mice[23] and humans.[31] As reported in mice,[15,21,23] we also identified a small population of human cells at the interface between the seminiferous tubes and the rete testis expressing *PAX8*, as well as Sertoli cell markers such as *AMH* and *SOX9*. This suggests that these cells harbor Sertoli-like features.

It remains a matter of debate whether the mesonephros contributes cells to the rete region of the human female and male gonads; however, mesonephric cells have been reported to contribute to myoid cells, fibroblasts, and endothelial cells to the testis.[3] Our results showed that estrogen sulfotransferase SULT1E1 is first expressed by male mesonephric stromal cells at 1T, but at 2T, it is also expressed by the rete testis mesenchyme and myoid compartment. In human adult testis, SULT1E1 has been specifically detected in Leydig cells.[57] Studies in mouse showed that mesonephric cells migrate to the testis and that part of the fetal Leydig cells are in fact derived from mesonephric stromal cells.[58,59] It remains to be investigated whether SULT1E1+ mesonephric stromal cells specifically contribute to human Leydig cells.

It is not surprising that WD, MTs, and MD all express known nephric lineage markers, such as *PAX2*, *PAX8*, and *LHX1*[60,61] because the human kidney (or metanephros) develops from an epithelial structure, the ureteric bud that sprouts from the caudal portion of the WD and penetrates a specific region in the intermediate mesoderm, the metanephric mesoderm.[4,62] Mutations in *PAX2* and *HNF1B*, found to be associated with urogenital abnormalities, can lead to Mayer-Rokitansky-Küster-Hauser (MRKH) syndrome that results in the underdevelopment or absence of the female reproductive tract.[63–65] MRKH can also be caused by mutations in other identified DEGs in the female reproductive tract, such as *LXH1* and *WNT9B*.[63–65] *WNT7A*, identified as a DEG in m.MD and found to be associated with genitourinary cancer, is also known to be involved in MD regression in XY mice, where *Wnt7a* mutation leads to a persistent MD.[66] In humans, persistent MD syndrome (PMDS) has so far only been associated with mutations in *AMH* and *AMHR2*.[67,68] Furthermore, we detected a clear involvement of the BMP and WNT pathways in the sex-specific development of the reproductive tract in humans in 1T, largely in agreement to what has been described in mice.[8] We also identified a clear involvement of *HOX* genes (*HOXB9*, *HOXA9*, and *HOXA10*) in the patterning of the reproductive tract at 1T, including the WD in both sexes. Interestingly, while HOX genes pattern the reproductive tract in humans and mice,[11,69] this also seems conserved in other vertebrates.[70]

In conclusion, we have analyzed the transcriptome of human fetal gonads and the mesonephros/reproductive tract from both sexes from 1T and 2T. We provided a comprehensive overview of the molecular profiles of the transition from fetal mesonephros to sex-specific reproductive tract. Notably, we have also identified mesonephric- and gonadal-specific stromal cells and epithelial cells. Finally, we identified the genes that may be related to morphogenesis and sex-specific development of the rete, WD, MD, and MTs. The provided datasets may serve as a valuable resource not only to shed light on the process of sexual differentiation in humans but also to provide insights into the genetic foundation underlying the development of the human reproductive ductal system.

Limitations of the study

Limitations of our study include the relatively small number of donors and developmental stages used for both single-cell sequencing and validation by immunofluorescence for both sexes.

STAR★METHODS

Detailed methods are provided in the online version of this paper and include the following:

- KEY RESOURCES TABLE
- RESOURCE AVAILABILITY
  - Lead contact
  - Materials availability
  - Data and code availability
- EXPERIMENTAL MODEL AND STUDY PARTICIPATION
  - Ethical statement and sample collection
- METHOD DETAILS
  - Preparation and sequencing of single-cell RNA-Seq libraries

(G) Heatmap showing the mean expression of 16 DEGs conserved between m.WD, m.MTs, and m.MD; and 15 DEGs conserved between f.WD, f.MTs, and f.MD in 1T male and female cell types of interest.
(H) Heatmap showing the mean expression of 97 DEGs unique of m.WD, 100 DEGs unique of f.WD, 63 DEGs unique of m.MTs, 105 DEGs unique of f.MTs, 57 DEGs unique of m.MD, and 42 DEGs unique of f.MD in 1T male and female cell types of interest.
(I) Selected GO terms (biological processes) and associated genes enriched in the pooled DEGs from m.WD, m.MTs, and m.MD, excluding female DEGs (top) and enriched in the pooled DEGs from f.WD, f.MTs, and f.MD, excluding male DEGs (bottom).
(J) Intersection between genes associated with specific diseases urogenital abnormalities, genitourinary cancer, and ambiguous genitalia and the total DEGs obtained for the 1T main cell types of interest (rete, WD, MD, and MTs) in both sexes.
See also Figure S6 and Tables S6 and S7.

- Association with disease-related genes
- Immunofluorescence
- Image analysis

- QUANTIFICATION AND STATISTICAL ANALYSIS
  - Processing and analysis of single cell RNA-Seq data
  - Differential gene expression analysis and GO term enrichment

SUPPLEMENTAL INFORMATION

Supplemental information can be found online at https://doi.org/10.1016/j.devcel.2024.01.006.

ACKNOWLEDGMENTS

We are very grateful to the staff of the Vrelinghuis, Utrecht and Gynaikon, Rotterdam for their efforts in obtaining the human fetal material, as well as the donors that have consented for the use of the material. In addition, we would like to thank D. Cats for helping with data analysis, S.M. Kiełbasa for assistance with the demultiplexing of the samples, M. Bialecka for assistance in the collection of the gonadal samples for sequencing, and M. Ferreira for discussions about the human rete testis. This work was supported by the European Research Council (ERC-CoG-2016-725722 OVOGROWTH) to J.T., S.M.C., I.M., X.F., and S.M.C.d.S.L.; the Dutch Research Council (NWO VICI-2018-91819642) to Y.W.C., S.H., and S.M.C.d.S.L.; the Dutch Organization for Health Research and Development (ZonMW PSIDER-2021-10250022120001) to T.v.d.H. and S.M.C.d.S.L.; the Novo Nordisk Foundation (reNEW NNF21CC0073729) to S.M.C., S.H., X.F., and S.M.C.d.S.L.); and the China Scholarship Council (CSC 201706320328) to X.F.

AUTHOR CONTRIBUTIONS

J.T., S.M.C., X.F., and S.M.C.d.S.L. conceived and designed the study. S.M.C., S.M.C.d.S.L., S.H., T.v.d.H., and L.E.v.d.M. collected samples. J.T., S.M.C., S.H., T.v.d.H., Y.W.C., and X.F. carried out experiments. J.T., X.F., H.M., and I.M. performed bioinformatic analyses. J.T., S.M.C., X.F., I.M., Y.W.C., S.H., T.v.d.H., H.M., L.E.v.d.M., and S.M.C.d.S.L. analyzed and interpreted data. J.T., S.M.C., X.F., and S.M.C.d.S.L. wrote the manuscript. All authors wrote, provided critical feedback, and approved the final version of the manuscript.

DECLARATION OF INTERESTS

The authors declare no competing interests.

Received: February 12, 2022
Revised: September 5, 2023
Accepted: January 8, 2024
Published: January 30, 2024

REFERENCES

1. Belle, M., Godefroy, D., Couly, G., Malone, S.A., Collier, F., Giacobini, P., and Chédotal, A. (2017). Tridimensional Visualization and Analysis of Early Human Development. Cell *169*, 161–173.e12.
2. Ludwig, K.S., and Landmann, L. (2005). Early development of the human mesonephros. Anat. Embryol. (Berl) *209*, 439–447.
3. Sainio, K. (2003). Development of the mesonephric kidney. In The Kidney, P. Vize, A.S. Woolf, and J. Bard, eds. (Elsevier), pp. 75–86.
4. Woolf, A.S., Winyard, P.J.D., Hermanns, M.M., and Welham, S.J.M. (2003). Maldevelopment of the human kidney and lower urinary tract: an overview. In The Kidney, P. Vize, A.S. Woolf, and J. Bard, eds. (Elsevier), pp. 337–393.
5. Jacob, M., Yusuf, F., and Jacob, H.J. (2012). Development, differentiation and derivatives of the Wolffian and Müllerian ducts. In The Human Embryo, S. Yamada and T. Takakuwa, eds. (IntechOpen), pp. 143–166. https://doi.org/10.5772/1209.
6. Yang, Y., Workman, S., and Wilson, M. (2018). The molecular pathways underlying early gonadal development. J. Mol. Endocrinol. https://doi.org/10.1530/JME-17-0314.
7. Massé, J., Watrin, T., Laurent, A., Deschamps, S., Guerrier, D., and Pellerin, I. (2009). The developing female genital tract: from genetics to epigenetics. Int. J. Dev. Biol. *53*, 411–424.
8. Zhao, F., and Yao, H.H. (2019). A tale of two tracts: history, current advances, and future directions of research on sexual differentiation of reproductive tractsdagger. Biol. Reprod. *101*, 602–616.
9. Allard, S., Adin, P., Gouédard, L., di Clemente, N., Josso, N., Orgebin-Crist, M.C., Picard, J.Y., and Xavier, F. (2000). Molecular mechanisms of hormone-mediated Mullerian duct regression: involvement of beta-catenin. Development *127*, 3349–3360.
10. Hess, R.A., Sharpe, R.M., and Hinton, B.T. (2021). Estrogens and development of the rete testis, efferent ductules, epididymis and vas deferens. Differentiation *118*, 41–71.
11. Joseph, A., Yao, H., and Hinton, B.T. (2009). Development and morphogenesis of the Wolffian/epididymal duct, more twists and turns. Dev. Biol. *325*, 6–14.
12. Combes, A.N., Lesieur, E., Harley, V.R., Sinclair, A.H., Little, M.H., Wilhelm, D., and Koopman, P. (2009). Three-dimensional visualization of testis cord morphogenesis, a novel tubulogenic mechanism in development. Dev. Dyn. *238*, 1033–1041.
13. Major, A.T., Estermann, M.A., and Smith, C.A. (2021). Anatomy, Endocrine Regulation, and Embryonic Development of the Rete Testis. Endocrinology *162*, bqab046.
14. Malolina, E.A., and Kulibin, A.Y. (2017). Rete testis and the adjacent seminiferous tubules during postembryonic development in mice. Russ. J. Dev. Biol. *48*, 385–392.
15. Malolina, E.A., and Kulibin, A.Y. (2019). The rete testis harbors Sertoli-like cells capable of expressing DMRT1. Reproduction *158*, 399–413.
16. McKey, J., Anbarci, D.N., Bunce, C., Ontiveros, A.E., Behringer, R.R., and Capel, B. (2022). Integration of mouse ovary morphogenesis with developmental dynamics of the oviduct, ovarian ligaments, and rete ovarii. eLife *11*, e81088.
17. Wenzel, J.G., and Odend'hal, S. (1985). The mammalian rete ovarii: a literature review. Cornell Vet. *75*, 411–425.
18. Kinnear, H.M., Tomaszewski, C.E., Chang, F.L., Moravek, M.B., Xu, M., Padmanabhan, V., and Shikanov, A. (2020). The ovarian stroma as a new frontier. Reproduction *160*, R25–R39.
19. Liu, C., Peng, J., Matzuk, M.M., and Yao, H.H. (2015). Lineage specification of ovarian theca cells requires multicellular interactions via oocyte and granulosa cells. Nat. Commun. *6*, 6934.
20. Svingen, T., François, M., Wilhelm, D., and Koopman, P. (2012). Three-dimensional imaging of Prox1-EGFP transgenic mouse gonads reveals divergent modes of lymphangiogenesis in the testis and ovary. PLoS One *7*, e52620.
21. Kulibin, A.Y., and Malolina, E.A. (2020). Formation of the rete testis during mouse embryonic development. Dev. Dyn. *249*, 1486–1499.
22. Chen, Y., Zheng, Y., Gao, Y., Lin, Z., Yang, S., Wang, T., Wang, Q., Xie, N., Hua, R., Liu, M., et al. (2018). Single-cell RNA-seq uncovers dynamic processes and critical regulators in mouse spermatogenesis. Cell Res. *28*, 879–896.
23. Mayère, C., Regard, V., Perea-Gomez, A., Bunce, C., Neirijnck, Y., Djari, C., Bellido-Carreras, N., Sararols, P., Reeves, R., Greenaway, S., et al. (2022). Origin, specification and differentiation of a rare supporting-like lineage in the developing mouse gonad. Sci. Adv. *8*, eabm0972.
24. Fan, X., Moustakas, I., Torrens-Juaneda, V., Lei, Q., Hamer, G., Louwe, L.A., Pilgram, G.S.K., Szuhai, K., Matorras, R., Eguizabal, C., et al. (2021). Transcriptional progression during meiotic prophase I reveals sex-specific features and X chromosome dynamics in human fetal female germline. PLoS Genet. *17*, e1009773.

25. Guo, J., Grow, E.J., Mlcochova, H., Maher, G.J., Lindskog, C., Nie, X., Guo, Y., Takei, Y., Yun, J., Cai, L., et al. (2018). The adult human testis transcriptional cell atlas. Cell Res. *28*, 1141–1157.

26. Guo, J., Sosa, E., Chitiashvili, T., Nie, X., Rojas, E.J., Oliver, E., DonorConnect, Plath, K., Hotaling, J.M., Stukenborg, J.B., et al. (2021). Single-cell analysis of the developing human testis reveals somatic niche cell specification and fetal germline stem cell establishment. Cell Stem Cell *28*, 764–778.e4.

27. Li, L., Dong, J., Yan, L., Yong, J., Liu, X., Hu, Y., Fan, X., Wu, X., Guo, H., Wang, X., et al. (2017). Single-Cell RNA-Seq Analysis Maps Development of Human Germline Cells and Gonadal Niche Interactions. Cell Stem Cell *20*, 858–873.e4.

28. Shami, A.N., Zheng, X., Munyoki, S.K., Ma, Q., Manske, G.L., Green, C.D., Sukhwani, M., Orwig, K.E., Li, J.Z., and Hammoud, S.S. (2020). Single-Cell RNA Sequencing of Human, Macaque, and Mouse Testes Uncovers Conserved and Divergent Features of Mammalian Spermatogenesis. Dev. Cell *54*, 529–547.e12.

29. Sohni, A., Tan, K., Song, H.W., Burow, D., de Rooij, D.G., Laurent, L., Hsieh, T.C., Rabah, R., Hammoud, S.S., Vicini, E., and Wilkinson, M.F. (2019). The Neonatal and Adult Human Testis Defined at the Single-Cell Level. Cell Rep. *26*, 1501–1517.e4.

30. Wang, M., Liu, X., Chang, G., Chen, Y., An, G., Yan, L., Gao, S., Xu, Y., Cui, Y., Dong, J., et al. (2018). Single-Cell RNA Sequencing Analysis Reveals Sequential Cell Fate Transition during Human Spermatogenesis. Cell Stem Cell *23*, 599–614.e4.

31. Garcia-Alonso, L., Lorenzi, V., Mazzeo, C.I., Alves-Lopes, J.P., Roberts, K., Sancho-Serra, C., Engelbert, J., Marečková, M., Gruhn, W.H., Botting, R.A., et al. (2022). Single-cell roadmap of human gonadal development. Nature *607*, 540–547.

32. Leir, S.H., Yin, S., Kerschner, J.L., Cosme, W., and Harris, A. (2020). An atlas of human proximal epididymis reveals cell-specific functions and distinct roles for CFTR. Life Sci. Alliance *3*, e202000744.

33. Ulrich, N.D., Shen, Y.C., Ma, Q., Yang, K., Hannum, D.F., Jones, A., Machlin, J., Randolph, J.F., Jr., Smith, Y.R., Schon, S.B., et al. (2022). Cellular heterogeneity of human fallopian tubes in normal and hydrosalpinx disease states identified using scRNA-seq. Dev. Cell *57*, 914–929.e7.

34. Bremmer, F., Ströbel, P., Jarry, H., Strecker, J., Gaisa, N., Strauß, A., Schweyer, S., Radzun, H.J., and Behnes, C.L. (2015). CK19 is a sensitive marker for yolk sac tumours of the testis. Diagn. Pathol. *10*, 7.

35. Tong, G.X., Memeo, L., Colarossi, C., Hamele-Bena, D., Magi-Galluzzi, C., Zhou, M., Lagana, S.M., Harik, L., Oliver-Krasinski, J.M., Mansukhani, M., et al. (2011). PAX8 and PAX2 immunostaining facilitates the diagnosis of primary epithelial neoplasms of the male genital tract. Am. J. Surg. Pathol. *35*, 1473–1483.

36. Boualia, S.K., Gaitan, Y., Tremblay, M., Sharma, R., Cardin, J., Kania, A., and Bouchard, M. (2013). A core transcriptional network composed of Pax2/8, Gata3 and Lim1 regulates key players of pro/mesonephros morphogenesis. Dev. Biol. *382*, 555–566.

37. Hochane, M., van den Berg, P.R., Fan, X., Bérenger-Currias, N., Adegeest, E., Bialecka, M., Nieveen, M., Menschaart, M., Chuva de Sousa Lopes, S.M., and Semrau, S. (2019). Single-cell transcriptomics reveals gene expression dynamics of human fetal kidney development. PLOS Biol. *17*, e3000152.

38. Ricci, G., and Catizone, A. (2014). Pleiotropic Activities of HGF/c-Met System in Testicular Physiology: Paracrine and Endocrine Implications. Front. Endocrinol. (Lausanne) *5*, 38.

39. Dinh, H.Q., Lin, X., Abbasi, F., Nameki, R., Haro, M., Olingy, C.E., Chang, H., Hernandez, L., Gayther, S.A., Wright, K.N., et al. (2021). Single-cell transcriptomics identifies gene expression networks driving differentiation and tumorigenesis in the human fallopian tube. Cell Rep. *35*, 108978.

40. Crosnier, C., Attié-Bitach, T., Encha-Razavi, F., Audollent, S., Soudy, F., Hadchouel, M., Meunier-Rotival, M., and Vekemans, M. (2000). JAGGED1 gene expression during human embryogenesis elucidates the wide phenotypic spectrum of Alagille syndrome. Hepatology *32*, 574–581.

41. Harneit, S., Paust, H.J., Mukhopadhyay, A.K., and Ergün, S. (1997). Localization of endothelin-1 and endothelin-receptors A and B in human epididymis. Mol. Hum. Reprod. *3*, 579–584.

42. Browne, J.A., Yang, R., Leir, S.H., Eggener, S.E., and Harris, A. (2016). Expression profiles of human epididymis epithelial cells reveal the functional diversity of caput, corpus and cauda regions. Mol. Hum. Reprod. *22*, 69–82.

43. Kumar, M., Syed, S.M., Taketo, M.M., and Tanwar, P.S. (2016). Epithelial Wnt/betacatenin signalling is essential for epididymal coiling. Dev. Biol. *412*, 234–249.

44. Battistone, M.A., Merkulova, M., Park, Y.J., Peralta, M.A., Gombar, F., Brown, D., and Breton, S. (2019). Unravelling purinergic regulation in the epididymis: activation of V-ATPase-dependent acidification by luminal ATP and adenosine. J. Physiol. *597*, 1957–1973.

45. Prabagaran, E., Bandivdekar, A.H., Dighe, V., and Raghavan, V.P. (2007). HOXBES2: a novel epididymal HOXB2 homeoprotein and its domain-specific association with spermatozoa. Biol. Reprod. *76*, 314–326.

46. Wong, J., Gasperoni, J., Fuller, J., Grommen, S.V.H., De Groef, B., Hogarth, C., and Dworkin, S. (2022). Crucial Convolution: Genetic and Molecular Mechanisms of Coiling during Epididymis Formation and Development in Embryogenesis. J. Dev. Biol. *10*, 25.

47. Tomaszewski, J., Joseph, A., Archambeault, D., and Yao, H.H. (2007). Essential roles of inhibin beta A in mouse epididymal coiling. Proc. Natl. Acad. Sci. USA *104*, 11322–11327.

48. Yi, M., Negishi, M., and Lee, S.J. (2021). Estrogen Sulfotransferase (SULT1E1): Its Molecular Regulation, Polymorphisms, and Clinical Perspectives. J. Pers. Med. *11*, 194.

49. Lue, Y., Swerdloff, R., Liu, Q., Mehta, H., Hikim, A.S., Lee, K.W., Jia, Y., Hwang, D., Cobb, L.J., Cohen, P., and Wang, C. (2010). Opposing roles of insulin-like growth factor binding protein 3 and humanin in the regulation of testicular germ cell apoptosis. Endocrinology *151*, 350–357.

50. Tholen, L.E., Hoenderop, J.G.J., and de Baaij, J.H.F. (2022). Mechanisms of ion transport regulation by HNF1beta in the kidney: beyond transcriptional regulation of channels and transporters. Pflugers Arch. *474*, 901–916.

51. Grote, D., Souabni, A., Busslinger, M., and Bouchard, M. (2006). Pax 2/8-regulated Gata 3 expression is necessary for morphogenesis and guidance of the nephric duct in the developing kidney. Development *133*, 53–61.

52. Labastie, M.C., Catala, M., Gregoire, J.M., and Peault, B. (1995). The GATA-3 gene is expressed during human kidney embryogenesis. Kidney Int. *47*, 1597–1603.

53. Estienne, A., and Price, C.A. (2018). The fibroblast growth factor 8 family in the female reproductive tract. Reproduction *155*, R53–R62.

54. Yerlikaya, G., Balendran, S., Pröstling, K., Reischer, T., Birner, P., Wenzl, R., Kuessel, L., Streubel, B., and Husslein, H. (2016). Comprehensive study of angiogenic factors in women with endometriosis compared to women without endometriosis. Eur. J. Obstet. Gynecol. Reprod. Biol. *204*, 88–98.

55. Peri, L.E., Koh, B.H., Ward, G.K., Bayguinov, Y., Hwang, S.J., Gould, T.W., Mullan, C.J., Sanders, K.M., and Ward, S.M. (2015). A novel class of interstitial cells in the mouse and monkey female reproductive tracts. Biol. Reprod. *92*, 102.

56. de Mello Santos, T., and Hinton, B.T. (2019). We, the developing rete testis, efferent ducts, and Wolffian duct, all hereby agree that we need to connect. Andrology *7*, 581–587.

57. Hartmann, K., Bennien, J., Wapelhorst, B., Bakhaus, K., Schumacher, V., Kliesch, S., Weidner, W., Bergmann, M., Geyer, J., and Fietz, D. (2016). Current insights into the sulfatase pathway in human testis and cultured Sertoli cells. Histochem. Cell Biol. *146*, 737–748.

58. Cunha, G.R., Cao, M., Aksel, S., Derpinghaus, A., and Baskin, L.S. (2023). Role of mesonephric contribution to mouse testicular development revisited. Differentiation *129*, 109–119.

59. DeFalco, T., Takahashi, S., and Capel, B. (2011). Two distinct origins for Leydig cell progenitors in the fetal testis. Dev. Biol. *352*, 14–26.

60. Bouchard, M., Souabni, A., Mandler, M., Neubüser, A., and Busslinger, M. (2002). Nephric lineage specification by Pax2 and Pax8. Genes Dev. *16*, 2958–2970.

61. Khoshdel Rad, N., Aghdami, N., and Moghadasali, R. (2020). Cellular and Molecular Mechanisms of Kidney Development: From the Embryo to the Kidney Organoid. Front. Cell Dev. Biol. *8*, 183.

62. Rumballe, B., Georgas, K., Wilkinson, L., and Little, M. (2010). Molecular anatomy of the kidney: what have we learned from gene expression and functional genomics? Pediatr. Nephrol. *25*, 1005–1016.

63. Chen, N., Zhao, S., Jolly, A., Wang, L., Pan, H., Yuan, J., Chen, S., Koch, A., Ma, C., Tian, W., et al. (2021). Perturbations of genes essential for Mullerian duct and Wolffian duct development in Mayer-Rokitansky-Kuster-Hauser syndrome. Am. J. Hum. Genet. *108*, 337–345.

64. Herlin, M.K., Petersen, M.B., and Brännström, M. (2020). Mayer-Rokitansky-Kuster-Hauser (MRKH) syndrome: a comprehensive update. Orphanet J. Rare Dis. *15*, 214.

65. Triantafyllidi, V.E., Mavrogianni, D., Kalampalikis, A., Litos, M., Roidi, S., and Michala, L. (2022). Identification of Genetic Causes in Mayer-Rokitansky-Kuster-Hauser (MRKH) Syndrome: A Systematic Review of the Literature. Children (Basel) *9*, 961.

66. Parr, B.A., and McMahon, A.P. (1998). Sexually dimorphic development of the mammalian reproductive tract requires Wnt-7a. Nature *395*, 707–710.

67. Alanazi, A.B., Aldhowayan, A., Almuhanna, M.M., and Alghamdi, A.M. (2022). Persistent Mullerian duct syndrome (PMDS): Case report and review of literature. Urol. Case Rep. *42*, 102031.

68. Fotiadou, A., Achilleos, O., Picard, J.Y., Lamprinou, Z., Passalides, A., and Vlachopapadopoulou, E.A. (2023). A novel mutation in the AMHR2 gene, resulting in persistent Mullerian duct syndrome presenting with bilateral cryptorchidism and obstructed inguinal hernia. J. Pediatr. Endocrinol. Metab. *36*, 890–894.

69. Podlasek, C.A., Seo, R.M., Clemens, J.Q., Ma, L., Maas, R.L., and Bushman, W. (1999). Hoxa-10 deficient male mice exhibit abnormal development of the accessory sex organs. Dev. Dyn. *214*, 1–12.

70. Major, A.T., Estermann, M.A., Roly, Z.Y., and Smith, C.A. (2022). An evo-devo perspective of the female reproductive tract. Biol. Reprod. *106*, 9–23.

71. Schindelin, J., Arganda-Carreras, I., Frise, E., Kaynig, V., Longair, M., Pietzsch, T., Preibisch, S., Rueden, C., Saalfeld, S., Schmid, B., et al. (2012). Fiji: an open-source platform for biological-image analysis. Nat. Methods *9*, 676–682.

72. Hao, Y., Hao, S., Andersen-Nissen, E., Mauck, W.M., 3rd, Zheng, S., Butler, A., Lee, M.J., Wilk, A.J., Darby, C., Zager, M., et al. (2021). Integrated analysis of multimodal single-cell data. Cell *184*, 3573–3587. https://doi.org/10.1016/j.cell.2021.04.048.

73. Wickham, H. (2016). ggplot2: Elegant Graphics for Data Analysis (New York: Springer-Verlag).

74. Blighe, K., Rana, S., and Lewis, M. (2021). EnhancedVolcano: Publication-ready volcano plots with enhanced colouring and labeling. R package version 1.10.0.

75. Yu, G., Wang, L.G., Yan, G.R., and He, Q.Y. (2015). DOSE: an R/Bioconductor package for disease ontology semantic and enrichment analysis. Bioinformatics *31*, 608–609. https://doi.org/10.1093/bioinformatics/btu684.

76. Pagès, H., Carlson, M., Falcon, S., and Li, N. (2021). AnnotationDbi: Manipulation of SQLite-based annotations in Bioconductor. R package version 1.54.1.

77. Zheng, G.X., Terry, J.M., Belgrader, P., Ryvkin, P., Bent, Z.W., Wilson, R., Ziraldo, S.B., Wheeler, T.D., McDermott, G.P., Zhu, J., et al. (2017). Massively parallel digital transcriptional profiling of single cells. Nat Commun *8*, 14049. https://doi.org/10.1038/ncomms14049.

78. Huang, Y., McCarthy, D.J., and Stegle, O. (2019). Vireo: Bayesian demultiplexing of pooled single-cell RNA-seq data without genotype reference. Genome Biol *20*, 273. https://doi.org/10.1186/s13059-019-1865-2.

79. Haghverdi, L., Lun, A.T.L., Morgan, M.D., and Marioni, J.C. (2018). Batch effects in single-cell RNA-sequencing data are corrected by matching mutual nearest neighbors. Nat Biotechnol *36*, 421–427. https://doi.org/10.1038/nbt.4091.

80. Gentleman, R., Carey, V.J., Huber, W., and Hahne, F. (2021). genefilter: genefilter: methods for filtering genes from high-throughput experiments. R package version 1.74.0.

81. Angerer, P., Haghverdi, L., Buttner, M., Theis, F.J., Marr, C., and Buettner, F. (2016). destiny: diffusion maps for large-scale single-cell data in R. Bioinformatics *32*, 1241–1243. https://doi.org/10.1093/bioinformatics/btv715.

82. Germain, P.L., Lun, A., Garcia Meixide, C., Macnair, W., and Robinson, M.D. (2021). Doublet identification in single-cell sequencing data using scDblFinder. F1000Res *10*, 979. https://doi.org/10.12688/f1000research.73600.2.

83. Van den Brink, S.C., Sage, F., Vertesy, A., Spanjaard, B., Peterson-Maduro, J., Baron, C.S., Robin, C., and van Oudenaarden, A. (2017). Single-cell sequencing reveals dissociation-induced gene expression in tissue subpopulations. Nat Methods *14*, 935–936. https://doi.org/10.1038/nmeth.4437.

STAR★METHODS

KEY RESOURCES TABLE

REAGENT or RESOURCE	SOURCE	IDENTIFIER
Antibodies		
Goat polyclonal anti-FOXL2 Dilution 1:200	Novus Biologicals	Cat# NB100-1277; RRID: AB_2106188
Rabbit monoclonal anti-KRT19 Dilution 1:100	Abcam	Cat# ab76539; RRID: AB_1523469
Mouse monoclonal anti-GATM Dilution 1:100	Abcam	Cat# ab119269; RRID: AB_10902241
Goat polyclonal anti-PODXL Dilution 1:150	R&D Systems	Cat# AF1658; RRID: AB_354920
Rabbit monoclonal anti-NR2F2 Dilution 1:250	Cell Signaling Technology	Cat# 6434S; RRID: AB_11220428
Mouse monoclonal anti-AMH Dilution 1:50	Bio-Rad	Cat# MCA2246; RRID: AB_2226471
Rabbit polyclonal anti-COLIV Dilution 1:50	Chemicon International	Cat# AB748; RRID: AB_2276468
Goat polyclonal anti-GATA2 Dilution 1:200	R&D Systems	Cat# AF2046; RRID: AB_355123
Goat polyclonal anti-DDX4 Dilution 1:500	R&D Systems	Cat# AF2030; RRID: AB_2277369
Mouse monoclonal anti-POU5F1 Dilution 1:200	Santa Cruz	Cat# sc-8628; RRID: AB_653551
Rabbit polyclonal anti-PAX8 Dilution 1:1000	Proteintech	Cat# 10336-1-AP; RRID: AB_2236705
Goat polyclonal anti-SOX17 Dilution1:200	R&D Systems	Cat# AF1924; RRID: AB_355060
Goat polyclonal anti-JAG1 Dilution1:50	Santa Cruz	Cat# sc-6011; RRID: AB_649689
Goat polyclonal anti-PAX2 Dilution1:100	R&D Systems	Cat# AF3364; RRID: AB_10889828
Rabbit polyclonal anti-PCP4 Dilution 1:50	Santa Cruz	Cat# sc-98549; RRID: AB_2251885
Mouse monoclonal anti-CDH2 Dilution 1:100	Sigma Aldrich	Cat# C3865; RRID: AB_262097
Rabbit polyclonal anti-WT1 Dilution 1:100	Abcam	Cat# ab89901; RRID: AB_2043201
Goat polyclonal anti-GATA3 Dilution 1:100	R&D Systems	Cat# AF2605; RRID: AB_2108571
Mouse monoclonal anti-GATA4 Dilution 1:100	Abcam	Cat# ab84593; RRID: AB_10670538
Rabbit polyclonal anti-PDGFRA Dilution 1:100	Cell Signaling Technology	Cat# 3164; RRID: AB_2162351
Goat polyclonal anti-SULT1E1 Dilution 1:100	R&D Systems	Cat# AF5545; RRID: AB_1964719
Mouse monoclonal anti-KRT7 Dilution 1:200	Thermo Fisher Scientific	Cat# MA5-11986; RRID: AB_10989596
Mouse monoclonal anti-panKRT, Dilution 1:100	DAKO	Cat# M351501; RRID: AB_2631307
Alexa Fluor 488 donkey anti-rabbit IgG Dilution 1:500	Life Technologies	Cat# A-21206; RRID: AB_2535792

(*Continued on next page*)

Continued

REAGENT or RESOURCE	SOURCE	IDENTIFIER
Alexa Fluor 488 donkey anti-mouse IgG Dilution 1:500	Life Technologies	Cat# A-21202; RRID: AB_141607
Alexa Fluor 594 donkey anti-mouse IgG Dilution 1:500	Life Technologies	Cat# A-21203; RRID: AB_141633
Alexa Fluor 594 donkey anti-goat IgG Dilution 1:500	Life Technologies	Cat# A-11058; RRID: AB_2534105
Alexa Fluor 647 donkey anti-goat IgG Dilution 1:500	Life Technologies	Cat# A-21447; RRID: AB_141844
Alexa Fluor 647 donkey anti-rabbit IgG Dilution 1:500	Life Technologies	Cat# A-31573; RRID: AB_2536183
7AAD Viability Staining Solution Dilution 1:100	BioLegend	Cat# 420403
Chemicals, peptides, and recombinant proteins		
4′,6-diamidino-2-phenylindole (DAPI)	Life Technologies	Cat# D3571
ProLong Gold Antifade Mountant	Life Technologies	Cat# P36930
0.9% NaCl solution	Apotheek AZL	Cat# 14557487
0.25% trypsin-EDTA	Life Technologies	Cat# 25200-056
Collagenase II	Thermo Fisher Scientific	Cat# 17101-015
DMEM/F12	Thermo Fisher Scientific	Cat# 11330-032
Advanced DMEM/F12	Thermo Fisher Scientific	Cat# 12634-010
Penicillin/Streptomycin	Invitrogen	Cat# 15070-063
L-Glutamine	Thermo Fisher Scientific	Cat# 25030-024
RNase-free DNase I	Qiagen	Cat# 79254
Fetal Calf Serum (FCS)	Biowest	Cat# S00F910002
BAMBANKER™ Serum-Free Cell Freezing Medium+10% DMSO	Nippon Genetics	Cat# BB01
Tween-20	Merck	Cat# 8.22184.0500
Triton X-100	Sigma-Aldrich	Cat# T8787
Bovine Serum Albumin (BSA) solution	Sigma-Aldrich	Cat# A8022
UltraPure 0.5M EDTA	Life Technologies	Cat# 15575020
EDTA	VWR	Cat# M101-1kg
Paraformaldehyde (PFA)	Merck	Cat# 1.04005.1000
Xylene	KLINIPATH	Cat# 4055–9005
Ethanol absolute	VWR	Cat# 83813.360
Citric acid	Sigma	Cat# 251275
TriSodium citrate dihydrate (trisodium citrate)	Merck	Cat# S1804
Trizma base (Tris)	Sigma-Aldrich	Cat# T6066
DPBS without calcium and magnesium	Thermo Fisher Scientific	Cat# 14040-133
Critical commercial assays		
Chromium single cell 3’ Reagent v2 kit	10x Genomics	Cat# PN-120237
Chromium Next GEM Single Cell 3’ HT Kit v3.1	10x Genomics	Cat# PN-1000348
Chromium Next GEM Chip M Single Cell Kit	10x Genomics	Cat# PN-1000349
Dual Index Kit TT Set A	10x Genomics	Cat# PN-1000215
Qubit Assay Kit	Invitrogen	Cat# Q33231
Biological samples		
1st trimester human samples	Abortion clinic Gynaikon, Rotterdam, the Netherlands	N/A
2nd trimester human samples	Abortion clinic Vrelinghuis, Utrecht, the Netherlands	N/A
3rd trimester human sample	Biobank Dept. Pathology, LUMC, the Netherlands	N/A

(*Continued on next page*)

Continued

REAGENT or RESOURCE	SOURCE	IDENTIFIER
Deposited Data		
Single cell RNA-seq dataset	This study	[Database]:[GSE181558]
Software and algorithms		
LAS X v3.7.4	Leica	https://www.leica-microsystems.com/products/microscope-software/p/leica-las-x-ls/
ZEN (blue edition) v3.2.0	ZEISS	https://www.zeiss.com/microscopy/int/products/microscope-software/zen-lite.html
ImageJ v1.53f51	Schindelin et al.[71]	https://imagej.net/ij/features.html
R v4.0.5/ v4.1.2	R Core Team (2021). R: A Language and Environment for Statistical Computing, Vienna, Austria.	http://www.R-project.org/.
Rstudio v2022.03	RStudio Team (2020). RStudio: Integrated Development for R. RStudio, PBC, Boston, MA.	http://www.rstudio.com/
Seurat v4.1.1/v4.3.0	Hao et al.[72]	http://satijalab.org/seurat/
ggplot2 v3.3.5	Wickham[73]	https://ggplot2.tidyverse.org/
EnhancedVolcano v1.10.0	Blighe et al.[74]	https://github.com/kevinblighe/EnhancedVolcano
DOSE v3.18.1	Yu et al.[75]	https://www.bioconductor.org/packages/devel/bioc/vignettes/DOSE/inst/doc/DOSE.html
AnnotationDbi v1.54.1	Pagès et al.[76]	https://github.com/Bioconductor/AnnotationDbi
Cell Ranger v2.1.1/ v6.0.2	Zheng et al.[77]	https://github.com/rsheets/cellranger
Vireo2 v0.2.3	Huang et al.[78]	https://github.com/single-cell-genetics/vireo
batchelor v1.6.0	Haghverdi et al.[79]	https://github.com/LTLA/batchelor
genefilter v1.74.0	Gentleman et al.[80]	https://github.com/Bioconductor/genefilter
destiny v3.8.1	Angerer et al.[81]	https://github.com/theislab/destiny
scDblFinder v1.11.4	Germain et al.[82]	https://github.com/plger/scDblFinder

RESOURCE AVAILABILITY

Lead contact

Further information and requests for resources and reagents should be directed to and will be fulfilled by the lead contact: Prof. Dr. Susana M. Chuva de Sousa Lopes (lopes@lumc.nl).

Materials availability

This study did not generate new unique reagents.

Data and code availability

The accession number for the RNA sequencing and processed data reported in this paper is Gene expression omnibus (GEO): GSE181558.

The code used in the manuscript is available on github: https://github.com/chuvalab/embryo_gonads (https://doi.org/10.5281/zenodo.10410673).

Images and single cell transcriptomics data are available for interrogation under 'expression viewer' and 'image atlas' at http://ovogrowth.net/.

EXPERIMENTAL MODEL AND STUDY PARTICIPATION

Ethical statement and sample collection

All experiments performed in this study were conformed to the Declaration of Helsinki for Medical Research involving Human Subjects and a letter of no objection was obtained from by the Medical Ethical Committee of the Leiden University Medical Center

(P08.087 and B21.052). First and second trimester human fetal material used in this study was obtained with informed consent from the donors, after elective abortions without medical indication. Paraffin sections of the 30WPF ovary and female reproductive tract were provided by the biobank of the Dept of Pathology of the Leiden University Medical Center.

The developmental age of the fetal samples was estimated in WPF by ultrasonography. The human fetal gonads, mesonephros and epididymis were dissected in 0.9% NaCl solution for further use.

METHOD DETAILS

Preparation and sequencing of single-cell RNA-Seq libraries

Human fetal gonads, mesonephros and epididymis were prepared for single cell RNA sequencing as previously described.[37] Briefly, human fetal gonads, mesonephros and epididymis were incubated overnight at 4°C in an enzyme mix solution (0.1% collagenase II in 0.25% trypsin-EDTA solution). The following day, the samples were centrifuged at 160xg for 3 minutes (min) and incubated in Advanced DMEM/F12 containing 1x Penicillin/Streptomycin, 1x L-Glutamine and 27.3IU/ml RNase-free DNase I, at 37°C for 30min to 1 hour. Next, the cell suspension was pipetted up and down for 1min and the enzyme activity was neutralized by adding 10% FCS. The samples were filtered through a 100μm cell strainer (Corning) and centrifuged at 160xg for 3min. The single cell suspension was cryopreserved in Bambanker and stored in liquid nitrogen until use.

The single cell suspensions were thawed and resuspended in FACS buffer (1% BSA and 2 mM UltraPure EDTA in DPBS without calcium and magnesium). The cell suspensions were filtered through the FACS tube strainer cap and treated with 7AAD on ice for 3 min. Live cells were sorted on a BD FACS Aria I (BD Biosciences) system, equipped with a 50μm nozzle, 405nm laser, a 695/40A long pass filter and BD FACSDiva 8.0.1 software. Cells were collected in 1% BSA in DMEM/F12 with 1x Penicillin/Streptomycin. The collected live cells were sent to the Leiden Genome Technology Center (LGTC) for library preparation using the 10x Genomics Chromium single cell 3' Reagent v2 kit or 10x Genomics Chromium single cell 3' Reagent v3.1 kit according to the manufacturers' instructions.[74] The quality and quantity of the cDNA library was determined using 2100 Bioanalyzer (Agilent, Santa Clara, CA, USA) and performing Qubit Assay (Q33231, Invitrogen) prior to sequencing on NovaSeq 6000 (Illumina, San Diego, CA, USA).

Association with disease-related genes

The gene lists associated with disease-terms "urogenital abnormalities, C0042063", "genitourinary cancer, C0751569" and "ambiguous genitalia, C0266362" were downloaded from DisGeNET v7.0. Each list of disease-related genes was intersected with all DEGs identified in 1T female and male MD, WD and MTs.

Immunofluorescence

Human material was fixed in 4% PFA overnight at 4°C in a rocking platform, washed in PBS and stored in 70% ethanol at 4°C. The tissue was embedded in paraffin, using a Shandon Excelsior Tissue processor (Thermo Scientific). With a RM2065 Microtome (Leica Instruments), paraffin blocks were sectioned and the sections (5μm thick) were transferred onto StarFrost slides (Knittel) and rested overnight at 37°C. Thereafter, the sections were deparaffinized in xylene (2x 10 min) and rehydrated in decreasing ethanol concentration steps (2x 100%, 90%, 80%, 70%) and finally washed in distilled water. Antigen retrieval was performed in a microwave for 12min at 98°C using 10mM Tris/1mM EDTA buffer (pH 9.0). Afterwards, the sections were cooled down to room temperature (RT), washed 2x in PBS for 5min, 1x in PBST (0.05% Tween-20 in PBS) for 5min and blocked using blocking buffer (1% BSA, 0.05% Tween-20 in PBS) in a humidified chamber for 1 hour at RT. Next, the sections were incubated with primary antibodies diluted in blocking buffer overnight at 4°C in a humidified chamber, washed twice in PBS and once in PBST (5min each wash) and incubated with secondary antibodies and DAPI diluted in blocking buffer, in a humidified chamber for 1 hour at RT. Sections were then washed twice in PBS, once in PBST and once in distilled water (5min each wash) at RT and mounted using ProLong Gold. All primary and secondary antibodies as well as the working dilutions used are listed in the key resources table.

Image analysis

Sections used for immunofluorescence were imaged on a Leica TCS SP8 confocal microscope (Leica) with LAS X software (Leica) using the HC PL APO 40x/1.40 oil objective. Overview scan of all slides were taken with ZEISS Axioscan 7 slide scanner (ZEISS Group). Acquired images were further analyzed with ImageJ software.

QUANTIFICATION AND STATISTICAL ANALYSIS

Processing and analysis of single cell RNA-Seq data

Raw RNA sequencing data of human fetal female and male gonads, mesonephros and reproductive tracts was initially processed using the Cell Ranger pipeline (v6.1.1). Reads were aligned to the human reference genome (GRCh38), transcriptome version GRCh38-2020-A. The R package Vireo (v0.2.3) was applied to assign cells to individuals based on the genetic variation. Afterwards, a Seurat-based workflow was used. Briefly, for quality control, cells expressing less than 750 or more than 7000 genes or having more than 50000 UMIs or with more than 10% of the total UMIs coming from mitochondrial genes were excluded from further analysis. Additionally, we also excluded cells with more than 6% of UMIs mapping to dissociation-induced genes.[83] Data was then normalized

using the NormalizeData function with the parameter scale.factor set to 50000. R package scDblFinder (v1.11.4) was used to detect doublets in the dataset which were excluded from further analysis. The top 2000 (default) highly variable features (genes) were selected with FindVariableFeatures function followed by Principal Component Analysis (PCA). To focus on cell type-specific differences in the datasets, batch effects between sequencing batches were corrected using the fastMNN function from R package batchelor (v1.6.0). The first 16 principal components (PCs) were used to calculate cell clusters for the male and female datasets, with the resolution parameter was set to 0.3 (Figures 2A and 5A). Differentially expressed genes (DEGs) for each cluster were calculated with function FindAllMarkers (only.pos = TRUE) and filtered with pct.1 > 0.6 and p_val_adj < 0.05 (Tables S1, S2, S3, S4, S5, S6, and S7). To perform sub-clustering, we first isolated the specific cluster(s) of interest using the subset function from Seurat, followed by the same workflow as above. For rete testis (mCL11) (Figures 3A and S3C; Table S2) and rete ovarii (fCL4) (Figures 6G, S5B, and S5C; Table S4) sub-clustering, 8 PCs with resolution 0.2 was applied. To sub-cluster mesonephric epithelial cells (male mCL7 and female fCL7) (Figures 7 and S6; Tables S6 and S7), 10 PCs and resolution 0.3 was applied.

Differential gene expression analysis and GO term enrichment

For differential expression analysis of rete testis in different age groups (7WPF, 9-12WPF and 16-18WPF) (Figures 3A, S3C, and S3D; Table S2), the subset function from Seurat was first applied to mCL11 to extract the three age groups and DEGs were calculated using the function FindAllMarkers (only.pos = TRUE) (Table S2). To identify DEGs of rete, WD, MTs and MD cells in 1T for each sex, we used the subset function, followed by FindAllMarkers (only.pos = TRUE) between male clusters (m.rete, m.WD, m.MTs, m.MD, and m.rest) and between female clusters (f.rete, f.WD, f.MTs, f.MD, and f.rest). DEGs obtained were further filtered using thresholds: pct.1>0.3, p_val_adj <0.05 and avg_log2FC >1. DEGs between male mmeCL3+mmeCL5 and mmeCL0+mmeCL1, and between female fmeCL1 and fmeCL0+fmeCL4 were calculated similarly and filtered using p_val_adj <0.001 and avg_log2FC >1. DEGs were annotated using the AnnotationDbi (v1.54.1) package and imported for GO term enrichment analysis using the enrichGO function from the DOSE (v3.18.1) package. The GO terms were called specifically for biological process and filtered for p_val_adj <0.05 (Figures 3D, 7I, S3I, and S5G).